

AD-A169 004

LG WAVE EXCITATION AND PROPAGATION IN PRESENCE OF ONE-
TWO AND THREE-DIMENSIONAL HETEROGENEITIES(U) SAINT
LOUIS UNIV MO R B HERRMANN 27 JAN 86 AFGL-TR-86-0025

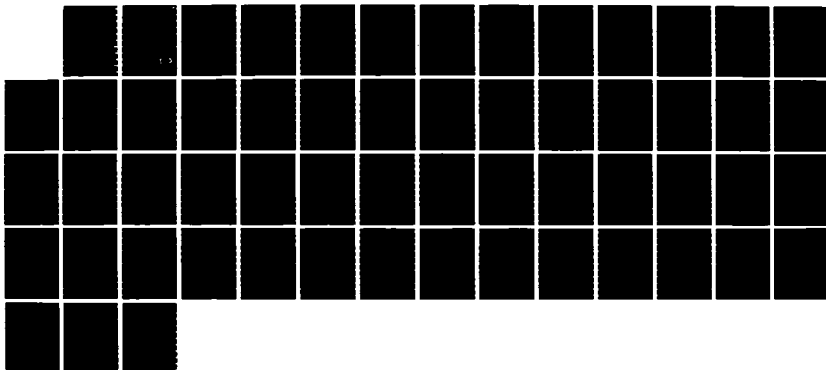
1/1

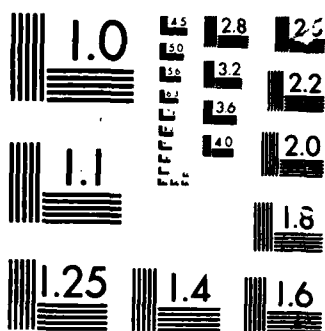
UNCLASSIFIED

F19628-85-K-0029

F/G 20/14

NL





UNIT 1

12

AFGL-TR-86-0025

Lg Wave Excitation and Propagation in
Presence of One-, Two, and Three-Dimensional
Heterogeneities

R. B. Herrmann

St. Louis University
221 North Grand Blvd
St. Louis, MO 63103

27 January 1986

Scientific Report No. 1

APPROVED FOR PUBLIC RELEASE; DISTRIBUTION UNLIMITED

DTIC
ELECTE
JUN 3 0 1986
S D
E

AIR FORCE GEOPHYSICS LABORATORY
AIR FORCE SYSTEMS COMMAND
UNITED STATES AIR FORCE
HANSCOM AIR FORCE BASE, MASSACHUSETTS 01731

86 6 30 020

AD-A169 004

DTIC FILE COPY

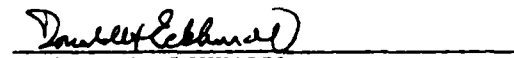
CONTRACTOR REPORTS

This technical report has been reviewed and is approved for publication.


JAMES F. LEWKOWICZ
Contract Manager


HENRY A. OSSING
Chief, Solid Earth Geophysics Branch

FOR THE COMMANDER


DONALD H. ECKHARDT
Director
Earth Sciences Division

This report has been reviewed by the ESD Public Affairs Office (PA) and is releasable to the National Technical Information Service (NTIS).

Qualified requesters may obtain additional copies from the Defense Technical Information Center. All others should apply to the National Technical Information Service.

If your address has changed, or if you wish to be removed from the mailing list, or if the addressee is no longer employed by your organization, please notify AFGL/DAA, Hanscom AFB, MA 01731. This will assist us in maintaining a current mailing list.

REPORT DOCUMENTATION PAGE

1a. REPORT SECURITY CLASSIFICATION unclassified			1b. RESTRICTIVE MARKINGS A169004	
2a. SECURITY CLASSIFICATION AUTHORITY			3. DISTRIBUTION/AVAILABILITY OF REPORT Approved for public release. Distribution unlimited.	
2b. DECLASSIFICATION/DOWNGRADING SCHEDULE				
4. PERFORMING ORGANIZATION REPORT NUMBER(S)			5. MONITORING ORGANIZATION REPORT NUMBER(S) AFGL-TR-86-0025	
6a. NAME OF PERFORMING ORGANIZATION Saint Louis University		6b. OFFICE SYMBOL (If applicable)	7a. NAME OF MONITORING ORGANIZATION Air Force Geophysics Laboratory	
6c. ADDRESS (City, State and ZIP Code) 221 North Grand Boulevard St. Louis, MO 63103			7b. ADDRESS (City, State and ZIP Code) Hanscom Air Force Base, MA 01731	
8a. NAME OF FUNDING/SPONSORING ORGANIZATION DARPA/DSO		8b. OFFICE SYMBOL (If applicable) GSD	9. PROCUREMENT INSTRUMENT IDENTIFICATION NUMBER F19628-85-K-0029	
8c. ADDRESS (City, State and ZIP Code) 1400 Wilson Blvd. Arlington, VA 22209			10. SOURCE OF FUNDING NOS.	
			PROGRAM ELEMENT NO.	PROJECT NO.
			61101F	5A10
11. TITLE (Include Security Classification) Lg Wave Excitation and Propagation in (OVER)			TASK NO.	WORK UNIT NO.
			DA	AO
12. PERSONAL AUTHOR(S) R.B. Herrmann				
13a. TYPE OF REPORT Scientific Report 1		13b. TIME COVERED FROM 4/1/85 TO 9/30/85	14. DATE OF REPORT (Yr., Mo., Day) 86 JAN 27	
15. PAGE COUNT 56				
16. SUPPLEMENTARY NOTATION				
17. CCSATI CODES			18. SUBJECT TERMS (Continue on reverse if necessary and identify by block number)	
FIELD	GROUP	SUB GR		
			Synthetic seismograms, numerical integration	
19. ABSTRACT (Continue on reverse if necessary and identify by block number)				
<p>In order to understand high frequency wave propagation, precise methods of generation of synthetic seismograms are required. This report examines the trapezoidal integration rule used by Bouchon (1981) to evaluate Hankel transforms of the Sommerfeld kernel. Numerical problems arise for integrals of some $J_0(kr)$ functions. A modification of the numerical integration technique, using a shifted mid-point rectangular rule rather than a trapezoidal rule alleviates some of the problem. For calibration of numerical integration techniques, the Haskell (1963) solution for point sources in a wholespace are extended.</p>				
20. DISTRIBUTION/AVAILABILITY OF ABSTRACT UNCLASSIFIED UNLIMITED <input type="checkbox"/> SAME AS RPT <input checked="" type="checkbox"/> DTIC USERS <input type="checkbox"/>			21. ABSTRACT SECURITY CLASSIFICATION Unclassified	
22a. NAME OF RESPONSIBLE INDIVIDUAL James F. Lewkowicz			22b. TELEPHONE NUMBER (Include Area Code) (617) 377-3028	22c. OFFICE SYMBOL AFGL/LWH

Cont. of Block 11:

Presence of One-, Two-, and Three-Dimensional Heterogeneities

TABLE OF CONTENTS

A Study of Wavenumber Integration Techniques	1
References	4
Appendix: Wholespace Solution	6
Time Histories	10
Numerical Examples	11

LIST OF FIGURES

1. Synthetic seismograms for the RDS component, using $\alpha = 0.0039$ and $L=100\text{km}$ 13
2. Synthetic seismograms for the RDS component, using $\alpha = 0.03125$ and $L=100\text{km}$ 14
3. Synthetic seismograms for the RDS component, using $\alpha = 0.03125$ and $L=200\text{km}$ 15
4. Synthetic seismograms for the RDS component, using $\alpha = 0.03125$ and $L=200\text{km}$, but using a reduced travel time display 16
5. Synthetic seismograms for the RDS component, using $\alpha = 0.03125$ and $L=200\text{km}$, a reduced travel time display, but using the shifted rectangular integration rule rather than the Buchon trapezoidal integration rule 17

Accession For	
NTIS GRA&I	<input checked="checked" type="checkbox"/>
DTIC TAB	<input type="checkbox"/>
Unannounced	<input type="checkbox"/>
Justification	
By _____	
Distribution/ _____	
Availability Codes	
Dist	Avail and/or Special
A-1	



A STUDY OF WAVENUMBER INTEGRATION TECHNIQUES

ABSTRACT

A detailed study is made of the Bouchon (1981) trapezoidal integration rule for evaluation of Sommerfeld integrals. A problem with non-propagating arrivals is found with integrands involving the zero order Bessel function. A mid-point rectangular integration rule is offered as a imperfect way to reduce this error. To test numerical evaluation of Hankel transforms, the Haskell (1963) wholespace solution is reformulated, and examples are given of the analytic, Bouchon numerical integration and mid-point numerical integration of the eight dislocation and two explosion Green's functions.

Bouchon (1981) discussed the application of a trapezoidal numerical integration rule to the evaluation of the Sommerfeld integral. The discussion followed previous work (Bouchon, 1979) on obtaining the solution for wave propagation due to a point source by evaluation of a two dimensional Fourier transform over the two spatial wave numbers. Because the behavior of numerical evaluation of Fourier transforms by the discrete Fourier transform technique is well known, Bouchon (1979) was able to show that a discrete two-dimensional trapezoidal rule yields a wave field corresponding to a distribution of point sources on a rectangular grid. Knowing this, it is easy to establish the wave number sampling interval required to yield seismograms uncontaminated by spatial aliasing.

Bouchon (1981) had the objective of specifying the wave number sampling criteria to avoid spurious arrivals due to spatial and temporal aliasing when a trapezoidal integration rule is applied to the Sommerfeld integral. Bouchon found that

$$\int_0^{\infty} F(k) J_0(kr) dk = \sum_{n=0}^{\infty} \epsilon_n F(k_n) J_0(k_n r) \Delta k, \quad (1)$$

where $\epsilon_0 = \frac{1}{2}$, $\epsilon_i = 1$, otherwise, $\Delta k = 2\pi/L$, $k_n = n\Delta k$, and $F(k)$ is the Sommerfeld kernel. The equality in equation (1) holds as long as the following two conditions hold:

$$L > 2r$$

$$[(L-r)^2 + z^2]^{\frac{1}{2}} > vt$$

where z is the vertical distance between the source and the receiver, r is the radial distance between the source and receiver, t is the maximum time for which a trace is to be generated, and v is the velocity of the wave, of the fastest wave if the problem has many arrivals. Outside this (r,t) window spurious arrivals are seen. In addition, since a discrete Fourier transform is used to invert (1) from the space-frequency to the space-time domain, Bouchon used a complex angular frequency given by $\omega - i\alpha$ to control the inherent periodicity in the time series.

Figures 1 - 3 illustrate the sensitivity of the resultant seismograms to the parameters L and α . The time history generated is that of the RDS Green's function (APPENDIX), for a point source at a depth of 10 km beneath the receiver. The medium parameters are given in the appendix. Figure 1 has $\alpha = 0.0039$ and $L = 100$ km, Figure 2 has $\alpha = 0.03125$ and $L = 100$ km, and Figure 3 has $\alpha = 0.03125$ and $L = 200$ km. A total of 64 seconds of time history are presented. The effect of the different values of α is not very apparent in these figures, since the later arrivals are of low amplitude to begin with. The difference is seen in the quietness of the traces prior to the first arrival, at 30 and 70 km for example, and in the occurrence of less ripple in Figure 2 than in Figure 1. A comparison of Figures 2 and 3 shows the effect of increasing L . The number of noise arrivals decreases.

Figure 4 uses the same parameters as Figure 3, except that a reduction velocity of 6.15 km/sec is used. All traces start at a time $t = 6.15 - 0.50$ seconds. At large distances, a

significant noise arrival overwhelms the expected solution. This noise arrival appears to be the integral of the expected waveshape in the far-field. It is present in Figures 1 - 3, and appears at a time corresponding to a non-causal arrival traveling the vertical distance between the source and the receiver. This noise is seen only in the integrals involving the $J_0(kr)$ Bessel function and corresponds to a $k=0$ contribution. The reason it appears worse in Figure 4 than in Figure 3, is that it wraps around to a later time, when reduced travel times are used, and is excessively exponentially increased when the time series is undamped. This points out the double edged effect of using complex frequency, in that the noise due to later arrivals can always be reduced, but an arrival earlier than the desired time window will be severely enhanced.

To understand the problem and also to appreciate the propagating noise terms, we return to the Bouchon (1981) development. Bouchon really showed that

$$\sum_{n=0}^{\infty} \epsilon_n F(k_n) J_m(k_n r) \Delta k = \int_0^{\infty} F(k) J_m(kr) dk \Delta k \sum_{n=-\infty}^{\infty} \delta(k-k_n) \quad (2a)$$

$$= \int_0^{\infty} F(k) J_m(kr) dk 2\pi \sum_{n=-\infty}^{\infty} \delta(kL-2n\pi) \quad (2b)$$

$$= \int_0^{\infty} F(k) J_m(kr) dk \sum_{n=-\infty}^{\infty} e^{inkL} \quad (2c)$$

$$= \int_0^{\infty} F(k) J_m(kr) dk \quad (2d)$$

$$+ \int_0^{\infty} F(k) J_m(kr) dk \sum_{n=1}^{\infty} 2\cos(nkL)$$

These are essentially equations (15-18) in Bouchon (1981), working backwards. We used the property of the Dirac distribution that $\delta(ax) = \delta(x)/|a|$. Bouchon further expanded (2d) to show its equivalence to contributions of concentric rings of sources with radii $L, 2L, 3L, \dots$, etc, about the point source. We note here that for large kr , we can use the asymptotic expansion of the Bessel function and a stationary phase approximation to show that the left hand side of (4) corresponds to an infinite set of arrivals in the (r,t) domain which are

$$g(r,z,t) + \left(\frac{L-r}{r} \right)^{1/2} \hat{g}(L-r,z,t) + \left(\frac{L+r}{r} \right)^{1/2} g(L+r,z,t) + \dots +$$

where the function \hat{g} is the Hilbert transform of g . The validity of this is seen by examining the noise arrivals in the Figures 1 - 4.

The functional form of (2d) is such that the equation is easily described in words! The trapezoidal integration rule is an approximation of the true integral, with the second term in (2d) being the error term. As seen the error term contributes propagating numerical noise. It is also apparent that the error term is indeterminate when $k=0$ because of the infinite summation. We have numerically evaluated the ten basic Green's functions for dislocation sources and explosive sources (Haskell, 1963; Haskell, 1964; Appendix of this paper) and found that the $k=0$ noise appeared only with the integrals containing the $J_0(kr)$ term. The kernel of the Sommerfeld integral, which is

$$\left(\frac{1}{R} \right) e^{i\omega R/v} = \int_0^{\infty} \left(\frac{k}{\nu_v} \right) e^{-\nu_v |z|} J_0(kr) dk, \quad (3a)$$

where

$$R^2 = r^2 + z^2$$

$$\nu_v^2 = k^2 - \left(\frac{\omega^2}{v^2} \right).$$

is zero at $k=0$, but evidently this is not enough to overcome the indeterminacy of the error term. On the other hand, the negative radial derivative of (3a),

$$\left(\frac{r}{R}\right)\left(\frac{1}{R^2} + \frac{i\omega}{Rv}\right)e^{-i\omega R/v} = \int_0^\infty \left(\frac{k^2}{\nu_v}\right)e^{-\nu_v |z|} J_1(kr) dk \quad (3b)$$

does not have such a noise arrival. The noise arrival is worst with the negative vertical derivative of (3a)

$$\left(\frac{z}{R}\right)\left(\frac{1}{R^2} + \frac{i\omega}{Rv}\right)e^{-i\omega R/v} = \int_0^\infty k e^{-\nu_v |z|} J_0(kr) dk \quad (3c)$$

at large distances, since the expected arrival decreases rapidly due to the radiation pattern term $\left(\frac{z}{R}\right)$ while the $k=0$ noise arrival does not.

A comparison of figures 2 and 3 shows that the $k=0$ noise term is reduced in amplitude by a factor of 4, with the same polarity, when Δk is decreased by a factor of 2, which is expected behavior for a trapezoidal integration rule (Abramowitz and Stegun, 1964). Consider for a moment the trapezoidal integration rule, first with sampling interval Δk and then with an interval $\Delta k/2$. The corresponding rules are

$$\int_0^\infty f(k) dk = \Delta k \left(\frac{1}{2} f_0 + f_1 + f_2 + \dots + \right) + O(\Delta k^2) \quad (4a)$$

and

$$\int_0^\infty f(k) dk = \Delta k \left(\frac{1}{2} f_0 + f_{\frac{1}{2}} + f_1 + f_{\frac{3}{2}} + f_2 + \dots + \right) + O(\Delta k^2/4) \quad (4b)$$

where $f_0 = f(n\Delta k)$. We note that (4b) is just the sum of (4a) and the mid-point rectangular integration rule

$$\int_0^\infty f(k) dk = \Delta k \left(f_{\frac{1}{2}} + f_{\frac{3}{2}} + \dots + \right) + O(\Delta k^2) \quad (4c)$$

Since the numerical experiment of Figures 2 and 3 showed that the $k=0$ noise was reduced by a factor of 4 when Δk is reduced by a factor of 2, this suggests that the synthetic generated using (4c) must have a $k=0$ noise arrival that is $\frac{3}{4}$ the size of that in (4a) so that (4b) yields a $k=0$ noise arrival that is $\frac{1}{4}$ that of (4a)!

The implication of this is that a shifted rectangular midpoint rule can be used to substantially reduce the $k=0$ noise arrival. In fact, we have found through numerical experiments that a numerical integration rule

$$\sum_{n=0}^\infty F(k_n) J_{n1}(k_n r) \Delta k \quad (5)$$

with

$$k_n = n\Delta k + 0.218\Delta k$$

works best with $\Delta k = 2\pi/L$.

Figure 5 consists of the same parameters as used to generate Figure 4, except that the shifted rectangular rule of (5) is used rather than the trapezoidal rule of (1). Numerical noise is still present at low frequencies, but at least the $k=0$ noise no longer overwhelms the expected signal at large distance. The remaining propagating noise can be reduced by using a larger value for L . As indicated above, a phase change is noted in the waveforms of the propagating noise arrivals, when they are compared to the corresponding arrivals in Figure 4.

For completeness, it is necessary to show that (5) is equivalent to the analytical integral within the Bouchon specified (r,t) window. Following (2) we obtain

$$\sum_{n=0}^{\infty} F(k_n) J_m(k_n r) \Delta k = \int_0^{\infty} F(k) J_m(kr) dk \Delta k \sum_{n=-\infty}^{\infty} \delta(k-k_n) \quad (6a)$$

$$\begin{aligned} &= \int_0^{\infty} F(k) J_m(kr) dk \\ &+ \int_0^{\infty} F(k) J_m(kr) dk \sum_{n=1}^{\infty} 2 \cos(n(k-k_0)L) \end{aligned} \quad (6b)$$

where we define $k_n = n\Delta k + k_0$. The only difference between (6b) and (2d) is the error term, which is no longer indeterminate when $k=0$. For large kr , the error term still represents propagating arrivals, with the inwardly and outwardly propagating arrivals differing by $\frac{\pi}{2}$ in phase, but now the outwardly propagating waves are also phase shifted with respect to the direct arrivals from the source.

The numerical integration rules used in (2) and (6) are simple cases of general Newton-Cotes integration rules. In numerical analysis, one typically is taught that a higher order Newton-Cotes formula, such as the Simpson rule, yields better estimates of the integral. This generalization is invalid when a wave propagation problem is being solved, as is done here. Using the same notation as used in (4), the Simpson rule would be

$$\begin{aligned} \int_0^{\infty} f(k) dk &= \left(\frac{\Delta k}{3} \right) (f_0 + 4f_1 + 2f_2 + 4f_3 + \dots) + O(\Delta k^4) \\ &= \left(\frac{2}{3} \right) \Delta k \left(\frac{1}{2} f_0 + f_1 + f_2 + \dots \right) \\ &+ \left(\frac{2}{3} \right) \Delta k (f_1 + f_3 + f_5 + \dots) \end{aligned} \quad (7)$$

which is recognized as a combination of a trapezoidal rule with sampling Δk with a midpoint rectangular rule with sampling $2\Delta k$. In evaluating wave propagation integrals of the Sommerfeld type, we would see more noise arrivals that in applying just the trapezoidal rule. In this case, an attempt at additional numerical accuracy backfired. A similar observation was made by Bakun and Eisenberg (1970) in a discussion of the numerical evaluation of the Fourier transform.

REFERENCES

- Abramowitz, M. and I. A. Stegun (1964). *Handbook of Mathematical Functions with Formulas, Graphs and Mathematical Tables*, National Bureau of Standards Applied Mathematics Series 55, U. S. Government Printing Office, Washington, DC.
- Bakun, W. H. and A. Eisenberg (1970). Fourier integrals and quadrature-introduced aliasing, *Bull. Seism. Soc. Am.* **60**, 1291-1296.
- Bouchon, M. (1979). Discrete wave number representation of elastic wave fields in three-dimensions, *J. Geophys. Res.* **84**, 3609-3614.
- Bouchon, M. (1981). A simple method to calculate Green's functions for elastic layered media, *Bull. Seism. Soc. Am.* **71**, 959-971.
- Brigham, E. O. (1974). *The Fast Fourier Transform*, Prentice-Hall, Englewood Cliffs, New Jersey. 252pp.
- Haskell, N. A. (1963). Radiation pattern of Rayleigh waves from a fault of arbitrary dip and

direction of motion in a homogeneous medium, *Bull. Seism. Soc. Am.* **53**, 619-642.

Haskell, N. A. (1964). Radiation pattern of surface waves from point sources in a multi-layered medium, *Bull. Seism. Soc. Am.* **54**, 377-393.

Herrmann, R. B. (1975). A student's guide to the use of P and S wave data for focal mechanism determination, *Earthquake Notes* **46**, 29-40.

Herrmann, R. B. (1979). SH-wave generation by dislocation sources - a numerical study, *Bull. Seism. Soc. Am.* **69**, 1-15.

Herrmann, R. B. and C. Y. Wang (1985). A comparison of synthetic seismograms, *Bull. Seism. Soc. Am.* **75**, 41-56.

Wang, C. Y. and R. B. Herrmann (1980). A numerical study of P-, SV-, and SH-wave generation in a plane layered medium, *Bull. Seism. Soc. Am.*, **70**, 1015-1036.

Department of Earth and Atmospheric Sciences
Saint Louis University
P. O. Box 8099 Laclede Station
St. Louis, MO 63158

APPENDIX: WHOLESAPCE SOLUTION

Haskell (1963) built the solution for the displacement field due to point couples in a wholespace by starting with the analytic solution for the displacement field due to a point force given in a cartesian coordinate system. Solutions for point single couples were obtained, and the solution was cast into a cylindrical coordinate system, through the use of partial derivatives of the Sommerfeld integral. Haskell (1964) extended the Haskell (1963) work to a layered halfspace, to include double-couple and dipole point forces. Because the Haskell (1963) work gives both the integrands of the Hankel transform as well as the analytical answer, the wholespace problem is the appropriate one to use for testing a numerical Hankel transform scheme. The equations below cast the Haskell (1963) derivations into the Green's functions for dislocation and explosive sources, given by Herrmann and Wang (1985). The Green's functions are defined as follow:

$$ZDD = \int_0^{\infty} F_1(k, \omega) J_0(kr) dk \quad (1a)$$

$$RDD = - \int_0^{\infty} F_2(k, \omega) J_1(kr) k dk \quad (1b)$$

$$ZDS = \int_0^{\infty} F_3(k, \omega) J_1(kr) dk \quad (1c)$$

$$RDS = \int_0^{\infty} F_4(k, \omega) J_0(kr) k dk \quad (1d)$$

$$TDS = \int_0^{\infty} F_9(k, \omega) J_0(kr) k dk \quad (1e)$$

$$- \frac{1}{r} \int_0^{\infty} [F_4(k, \omega) + F_9(k, \omega)] J_1(kr) dk$$

$$ZSS = \int_0^{\infty} F_8(k, \omega) J_2(kr) dk \quad (1f)$$

$$RSS = \int_0^{\infty} F_6(k, \omega) J_1(kr) k dk \quad (1g)$$

$$- \frac{2}{r} \int_0^{\infty} [F_6(k, \omega) + F_{10}(k, \omega)] J_2(kr) dk$$

$$TSS = \int_0^{\infty} F_{10}(k, \omega) J_1(kr) k dk \quad (1h)$$

$$- \frac{2}{r} \int_0^{\infty} [F_8(k, \omega) + F_{10}(k, \omega)] J_2(kr) dk$$

$$ZEP = \int_0^{\infty} F_7(k, \omega) J_0(kr) dk \quad (1i)$$

$$REP = - \int_0^{\infty} F_8(k, \omega) J_1(kr) k dk \quad (1j)$$

For an arbitrarily oriented double couple without moment source model with vector $\mathbf{n} = (n_1, n_2, n_3)$ normal to the fault and $\mathbf{f} = (f_1, f_2, f_3)$ in the direction of the dislocation (Haskell, 1963; Haskell, 1964), equation (11) of Wang and Herrmann (1980) for the Fourier transformed

displacements at the free surface at a distance r from the origin becomes

$$\begin{aligned} u_z(r, 0, \omega) = & ZSS[(f_1 n_1 - f_2 n_2) \cos 2\varphi + (f_1 n_2 + f_2 n_1) \sin 2\varphi] \\ & + ZDS[(f_1 n_3 + f_3 n_1) \cos \varphi + (f_2 n_3 + f_3 n_2) \sin \varphi] \\ & + ZDD[f_3 n_3] \end{aligned} \quad (2a)$$

$$\begin{aligned} u_r(r, 0, \omega) = & RSS[(f_1 n_1 - f_2 n_2) \cos 2\varphi + (f_1 n_2 + f_2 n_1) \sin 2\varphi] \\ & + RDS[(f_1 n_3 + f_3 n_1) \cos \varphi + (f_2 n_3 + f_3 n_2) \sin \varphi] \\ & + RDD[f_3 n_3] \end{aligned} \quad (2b)$$

$$\begin{aligned} u_\varphi(r, 0, \omega) = & TSS[(f_1 n_1 - f_2 n_2) \sin 2\varphi - (f_1 n_2 + f_2 n_1) \cos 2\varphi] \\ & + TDS[(f_1 n_2 + f_3 n_1) \sin \varphi - (f_2 n_3 + f_3 n_2) \cos \varphi] \end{aligned} \quad (2c)$$

Explicit expressions for the $F_j(k, \omega)$ functions for a point source buried at a depth h beneath the source in a wholespace with compressional velocity, α , shear velocity, β , and density, ρ , are derived from Haskell (1963, 1964) as follow:

Defining

$$\nu_\alpha = \begin{cases} \sqrt{k^2 - k_\alpha^2} & k \geq k_\alpha \\ i\sqrt{k_\alpha^2 - k^2} & k < k_\alpha \end{cases}$$

and

$$\nu_\beta = \begin{cases} \sqrt{k^2 - k_\beta^2} & k \geq k_\beta \\ i\sqrt{k_\beta^2 - k^2} & k < k_\beta \end{cases}$$

we have

$$F_1(k, \omega) = \frac{k}{4\pi\rho\omega^2} [(2k_\alpha^2 - 3k^2)e^{-\nu_\alpha h} + 3k^2 e^{-\nu_\beta h}] \quad (3a)$$

$$F_2(k, \omega) = \frac{-k}{4\pi\rho\omega^2} [(2k_\alpha^2 - 3k^2) \frac{e^{-\nu_\alpha h}}{\nu_\alpha} + 3\nu_\beta e^{-\nu_\beta h}] \quad (3b)$$

$$F_3(k, \omega) = \frac{k^2}{4\pi\rho\omega^2} [2\nu_\alpha e^{-\nu_\alpha h} - (2k^2 - k_\beta^2) \frac{e^{-\nu_\beta h}}{\nu_\beta}] \quad (3c)$$

$$F_4(k, \omega) = \frac{-1}{4\pi\rho\omega^2} [2k^2 e^{-\nu_\alpha h} - (2k^2 - k_\beta^2) e^{-\nu_\beta h}] \quad (3d)$$

$$F_5(k, \omega) = \frac{k^3}{4\pi\rho\omega^2} [e^{-\nu_\alpha h} - e^{-\nu_\beta h}] \quad (3e)$$

$$F_6(k, \omega) = \frac{k}{4\pi\rho\omega^2} [\frac{k^2}{\nu_\alpha} e^{-\nu_\alpha h} - \nu_\beta e^{-\nu_\beta h}] \quad (3f)$$

$$F_7(k, \omega) = \frac{k}{4\pi\rho\alpha^2} e^{-\nu_\alpha h} \quad (3g)$$

$$F_8(k, \omega) = \frac{-k}{4\pi\rho\alpha^2\nu_\alpha} e^{-\nu_\alpha h} \quad (3h)$$

$$F_9(k, \omega) = \frac{1}{4\pi\rho\beta^2} e^{-\nu_\beta h} \quad (3i)$$

$$F_{10}(k, \omega) = \frac{-k}{4\pi\rho\beta^2\nu_\beta} e^{-\nu_\beta h} \quad (3j)$$

The vertical displacement u_z is positive upward, the radial displacement is positive away from the source, and the tangential displacement u_ϕ is positive in a direction clockwise from north. The vectors \mathbf{n} and \mathbf{f} are still defined in a local coordinate system at the source in which the cartesian axes are in the north, east and downward directions. Following Herrmann (1975) the components of these vectors can be expressed in terms of the fault plane parameters of strike, dip and slip. The strike, ϕ_f , is measured clockwise from north, the dip, d_f , is measured in a positive sense from the horizontal direction perpendicular to strike, and the slip, λ_f , is measured on the fault plane in a counterclockwise sense from the horizontal direction of strike. With these conventions, all possible fault planes are encompassed by the ranges in the angles of $0^\circ \leq \phi_f < 360^\circ$, $0^\circ \leq d_f \leq 90^\circ$, and $-180^\circ \leq \lambda_f < 180^\circ$. With this notation, the sense of P-wave first motion at the center of the focal sphere is positive for positive values of λ_f and negative for negative values. The components of the vectors are

$$f_1 = \cos\lambda_f \cos\phi_f + \sin\lambda_f \cos d_f \sin\phi_f$$

$$f_2 = \cos\lambda_f \sin\phi_f - \sin\lambda_f \cos d_f \cos\phi_f$$

$$f_3 = -\sin\lambda_f \sin d_f$$

$$n_1 = -\sin\phi_f \sin d_f$$

$$n_2 = \cos\phi_f \sin d_f$$

$$n_3 = -\cos d_f$$

Following Haskell (1963), the analytic closed form solutions corresponding to (1a) to (1j) are

$$ZDD = \frac{1}{4\pi\rho\omega^2} \left[3 \frac{\partial^3 F_\alpha}{\partial z^3} + k_\alpha^2 \frac{\partial F_\alpha}{\partial z} - 3 \frac{\partial^3 F_\beta}{\partial z^3} - 3k_\beta^2 \frac{\partial F_\beta}{\partial z} \right] \quad (4a)$$

$$RDD = \frac{1}{4\pi\rho\omega^2} \left[3 \frac{\partial^3 F_\alpha}{\partial z^2 \partial r} - 3 \frac{\partial^3 F_\beta}{\partial z^2 \partial r} + k_\alpha^2 \frac{\partial F_\alpha}{\partial r} \right] \quad (4b)$$

$$ZDS = \frac{-1}{4\pi\rho\omega^2} \left[2 \frac{\partial^3 F_\alpha}{\partial z^2 \partial r} - 2 \frac{\partial^3 F_\beta}{\partial z^2 \partial r} - k_\beta^2 \frac{\partial F_\beta}{\partial r} \right] \quad (4c)$$

$$RDS = \frac{-1}{4\pi\rho\omega^2} \left[2 \frac{\partial^3 F_\alpha}{\partial r^2 \partial z} - 2 \frac{\partial^3 F_\beta}{\partial r^2 \partial z} - k_\beta^2 \frac{\partial F_\beta}{\partial z} \right] \quad (4d)$$

$$TDS = \frac{1}{4\pi\rho\omega^2} \left[\frac{2}{r} \left(\frac{\partial^2 F_\alpha}{\partial r \partial z} - \frac{\partial^2 F_\beta}{\partial r \partial z} \right) - k_\beta^2 \frac{\partial F_\beta}{\partial z} \right] \quad (4e)$$

$$ZSS = \frac{1}{4\pi\rho\omega^2} \left[2 \frac{\partial^3 F_\alpha}{\partial r^2 \partial z} + \frac{\partial^3 F_\alpha}{\partial z^3} + k_\alpha^2 \frac{\partial F_\alpha}{\partial z} - 2 \frac{\partial^3 F_\beta}{\partial r^2 \partial z} - \frac{\partial^3 F_\beta}{\partial z^3} - k_\beta^2 \frac{\partial F_\beta}{\partial z} \right] \quad (4f)$$

$$RSS = \frac{1}{4\pi\rho\omega^2} \left[2 \frac{\partial^3 F_\alpha}{\partial r^3} + \frac{\partial^3 F_\alpha}{\partial z^2 \partial r} + k_\alpha^2 \frac{\partial F_\alpha}{\partial r} - 2 \frac{\partial^3 F_\beta}{\partial r^3} - \frac{\partial^3 F_\beta}{\partial z^2 \partial r} - 2k_\beta^2 \frac{\partial F_\beta}{\partial r} \right] \quad (4g)$$

$$TSS = \frac{1}{4\pi\rho\omega^2} \left[2 \frac{\partial^3 F_\alpha}{\partial r^3} + 2 \frac{\partial^3 F_\alpha}{\partial z^2 \partial r} + 2k_\alpha^2 \frac{\partial F_\alpha}{\partial r} - 2 \frac{\partial^3 F_\beta}{\partial r^3} - 2 \frac{\partial^3 F_\beta}{\partial z^2 \partial r} - k_\beta^2 \frac{\partial F_\beta}{\partial r} \right] \quad (4h)$$

$$ZEP = \frac{-1}{4\pi\rho\alpha^2} \frac{\partial F_\alpha}{\partial z} \quad (4i)$$

$$REP = \frac{-1}{4\pi\rho\alpha^2} \frac{\partial F_\beta}{\partial r} \quad (4j)$$

The function F_v is the Sommerfeld integral,

$$\frac{1}{R} e^{\frac{-i\omega R}{v}} = \int_0^\infty \frac{k}{\nu_v} e^{-\nu_v h} J_0(kr) dk$$

where

$$R^2 = r^2 + h^2$$

and

$$\nu_v^2 = k^2 - \frac{\omega^2}{v^2}$$

The specific expressions for the partial derivatives of the Sommerfeld integral are

$$\frac{\partial F_v}{\partial z} = -e^{\frac{-i\omega R}{v}} \left[\frac{h}{R^3} + \left(\frac{i\omega}{v} \right) \frac{h}{R^2} \right]$$

$$\frac{\partial F_v}{\partial r} = -e^{\frac{-i\omega R}{v}} \left[\frac{r}{R^3} + \left(\frac{i\omega}{v} \right) \frac{r}{R^2} \right]$$

$$\frac{\partial^2 F_v}{\partial r \partial z} = -e^{\frac{-i\omega R}{v}} \left[\left(\frac{-3rz}{R^5} \right) + \left(\frac{i\omega}{v} \right) \left(\frac{-3rz}{R^4} \right) + \left(\frac{i\omega}{v} \right)^2 \left(\frac{-rz}{R^3} \right) \right]$$

$$\frac{\partial^3 F_v}{\partial r^3} = -e^{\frac{-i\omega R}{v}} \left[\left(\frac{-9r}{R^5} + \frac{15r^3}{R^7} \right) + \left(\frac{i\omega}{v} \right) \left(\frac{-9r}{R^4} + \frac{15r^3}{R^6} \right) + \left(\frac{i\omega}{v} \right)^2 \left(\frac{-3r}{R^3} + \frac{6r^3}{R^5} \right) + \left(\frac{i\omega}{v} \right)^3 \left(\frac{r^3}{R^4} \right) \right]$$

$$\frac{\partial^3 F_v}{\partial z^3} = -e^{\frac{-i\omega R}{v}} \left[\left(\frac{-9h}{R^5} + \frac{15h^3}{R^7} \right) + \left(\frac{i\omega}{v} \right) \left(\frac{-9h}{R^4} + \frac{15h^3}{R^6} \right) + \left(\frac{i\omega}{v} \right)^2 \left(\frac{-3h}{R^3} + \frac{6h^3}{R^5} \right) + \left(\frac{i\omega}{v} \right)^3 \left(\frac{h^3}{R^4} \right) \right]$$

$$\frac{\partial^3 F_v}{\partial r^2 \partial z} = -e^{\frac{-i\omega R}{v}} \left[\left(\frac{-3h}{R^5} + \frac{15r^2 z}{R^7} \right) + \left(\frac{i\omega}{v} \right) \left(\frac{-3h}{R^4} + \frac{15r^2 z}{R^6} \right) + \left(\frac{i\omega}{v} \right)^2 \left(\frac{-h}{R^3} + \frac{6r^2 z}{R^5} \right) + \left(\frac{i\omega}{v} \right)^3 \left(\frac{r^2 z}{R^4} \right) \right]$$

$$\frac{\partial^3 F_v}{\partial z^2 \partial r} = -e^{-\frac{i\omega R}{v}} \left[\left(\frac{-3r}{R^5} + \frac{15rz^2}{R^7} \right) + \left(\frac{i\omega}{v} \right) \left(\frac{-3r}{R^4} + \frac{15rz^2}{R^6} \right) + \left(\frac{i\omega}{v} \right)^2 \left(\frac{-1}{R^3} + \frac{6rz^2}{R^5} \right) + \left(\frac{i\omega}{v} \right)^3 \left(\frac{rz^2}{R^4} \right) \right]$$

TIME HISTORIES

Following Wang and Herrmann (1980), the following convention is used to define the Fourier transform $H(f)$ of the time series $h(t)$:

$$H(f) = \int_{-\infty}^{\infty} h(t) \exp(i2\pi ft) dt \quad (5)$$

This integral is approximated by a Discrete Fourier Transform in its Fast Fourier Transform implementation (Brigham, 1974).

To generate synthetic seismograms, the following source time function is used:

$$2\pi s(t) = \begin{cases} 0 & t \leq 0 \\ \frac{1}{2}(t/\tau)^2 & 0 < t \leq \tau \\ -\frac{1}{2}(t/\tau)^2 + 2(t/\tau) - 1 & \tau \leq t \leq 3\tau \\ \frac{1}{2}(t/\tau)^2 - 4(t/\tau) + 8 & 3\tau < t \leq 4\tau \\ 0 & t > 4\tau \end{cases} \quad (6)$$

This time function has a unit area. In addition, it has spectral zeros at certain frequencies. If $\tau = M\Delta t$, where M is some power of two, then spectral zeros are at frequencies $f_N, f_N/2, f_N/4, \dots, f_N/(2M)$, where f_N is the Nyquist frequency defined as $f_N = \frac{1}{2\Delta t}$, and N is also a power of 2. By choosing τ and Δt such that one of the spectral zeros occurs at the Nyquist frequency, the pulses can be synthesized and propagated through the model without the rippling introduced by an arbitrary, sharp high frequency spectral cutoff.

The synthetic seismograms are presented to show the effect of using the trapezoidal and mid-point rectangular numerical integration rules. The three sets of figures correspond to the evaluation of (1) for a wholespace. To provide a uniform basis of comparison, the seismic moment is fixed at a value of $1.0E+20$ dyne-cm, the duration parameter τ is set to 0.5 seconds, and the depth is fixed at a constant value of 10 km. The velocities are $\alpha=6.15$ km/sec and $\beta=3.55$ km/sec and the density is $\rho=2.8$ gm/cm³. A 256 point time series is synthesized using $\Delta t=0.25$ sec. Velocity time histories with units of cm/sec are generated. A causal $Q_\alpha = Q_\beta = 10000$ is used, but these are so large that they do not affect the results displayed. A time domain damping factor is used to reduce the discrete Fourier transform periodicity, which corresponds to replacing all occurrences of ω in the frequency domain by $\omega - i0.046875$. All resultant time series have been undamped.

An important aspect of the computations concerns the upper limit used in the Hankel transform. Obviously, a $KMAX = \infty$ is out of the question. Fortunately the integrands become small for large k due to the exponential decay terms, except, when the depth is zero. We take

$$KMAX = \max[FAC k_{min}, \frac{6}{h}]$$

where FAC is taken to be 3 in Figures 1-5 and 2 in the Figures in this appendix. The choice of two values controls special computations to ensure the proper computations of the low frequency contributions to the time history. Basically, an asymptotic expansion is used in this case to determine the contribution from $k=KMAX$ to $k=\infty$. Too large a value for FAC will require too many computations without much discernible difference in the high frequency synthetics, while too low a value will introduce significant low frequency errors in the time series.

NUMERICAL EXAMPLES

The first set of figures, "whom" gives the analytic solution using equation (4). A reduced travel time plot with initial time given by $t = -1.01 + r/6.15$ seconds, where r is the epicentral distance. The correspondence between the identifier JSRC and the specific Green's function is as follows:

JSRC	Green's Function
1	ZDD
2	RDD
3	ZDS
4	RDS
5	TDS
6	ZSS
7	RSS
8	TSS
9	ZEP
10	REP

The Green's functions show the P-wave and S-wave arrivals expected at large distances. The S-wave arrival on the RDD and RSS components has a waveform that is an integral of the expected far-field arrival, the corresponding shape of the P-wave.

The second set of figures, "W1000T0.00000", is the result of the numerical evaluation of the Hankel transforms using the Bouchon trapezoidal rule. An $L=1000$ km was used. The $k=0$ noise is very apparent on the ZDD, RDS, TDS and ZEP traces. This noise arrival also demonstrates the periodicity of the discrete Fourier transform as well as the problems with using complex frequency. Propagating noise arrivals are seen in the traces beyond 300 km, because the criteria relating L , r , z , v and t_{max} in equation (1) are no longer satisfied. To eliminate these, we need only make L somewhat larger. Nothing of value should be expected of the trace at 500 km because the direct and first inwardly propagating noise arrival superimpose. At this distance, the inequalities of the Bouchon analysis, equation (1), are violated.

the last set of figures, "W1000T0.21739", corresponds to the use of the mid-point rule (5) with $k_0 = 0.21739\Delta k$. As designed, the $k=0$ noise arrival is significantly reduced, although some low frequency numerical noise is introduced at large distance. The difference in the integration rules is most readily apparent in the TDS and ZEP time histories.

FIGURE CAPTIONS

- Fig. 1. Synthetic seismograms for the RDS component, using $\alpha=0.0039$ and $L=100\text{km}$.
- Fig. 2. Synthetic seismograms for the RDS component, using $\alpha=0.03125$ and $L=100\text{km}$.
- Fig. 3. Synthetic seismograms for the RDS component, using $\alpha=0.03125$ and $L=200\text{km}$.
- Fig. 4. Synthetic seismograms for the RDS component, using $\alpha=0.03125$ and $L=200\text{km}$, but using a reduced travel time display.
- Fig. 5. Synthetic seismograms for the RDS component, using $\alpha=0.03125$ and $L=200\text{km}$, a reduced travel time display, but using the shifted rectangular integration rule rather than the Bouchon trapezoidal integration rule.

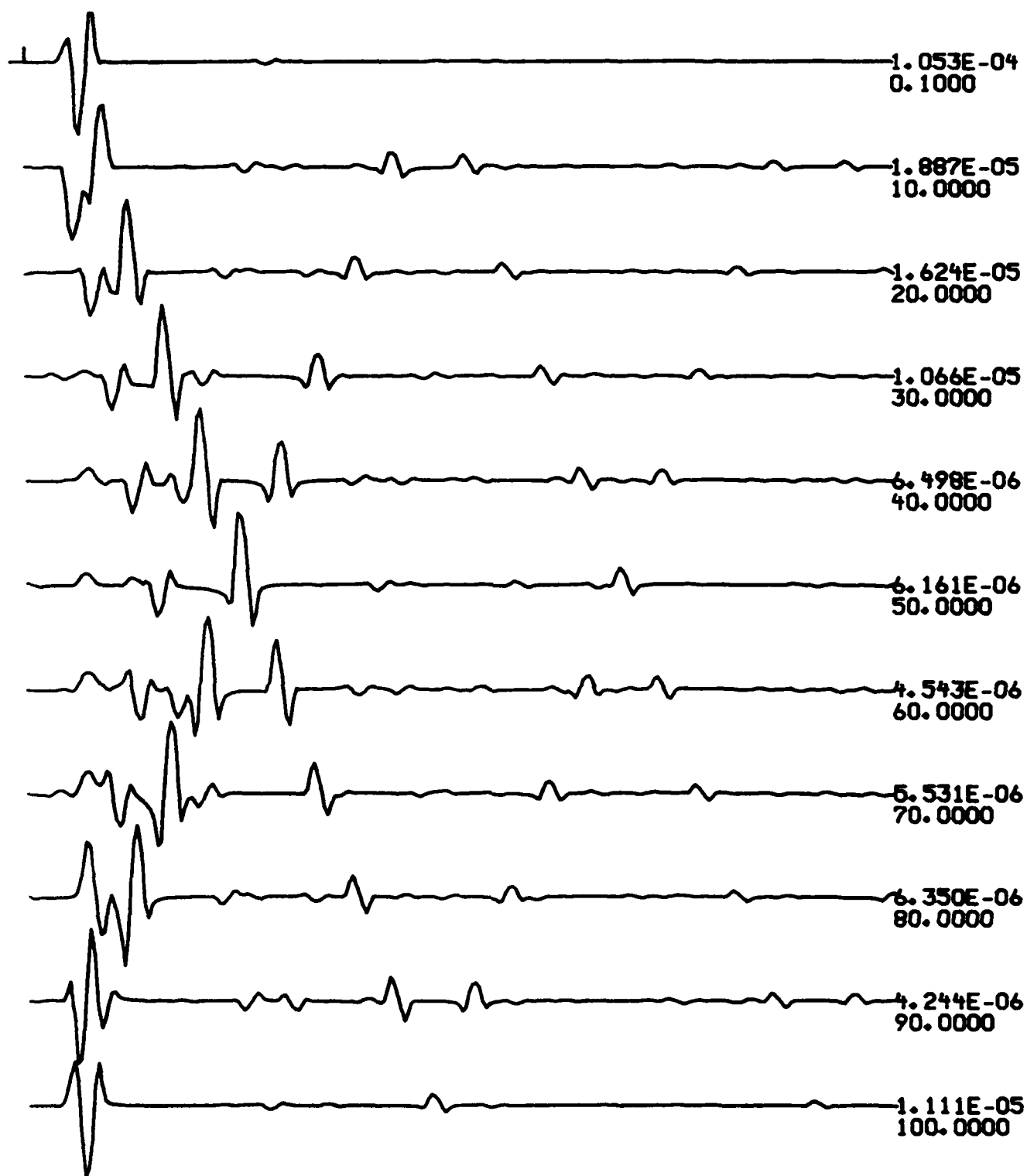
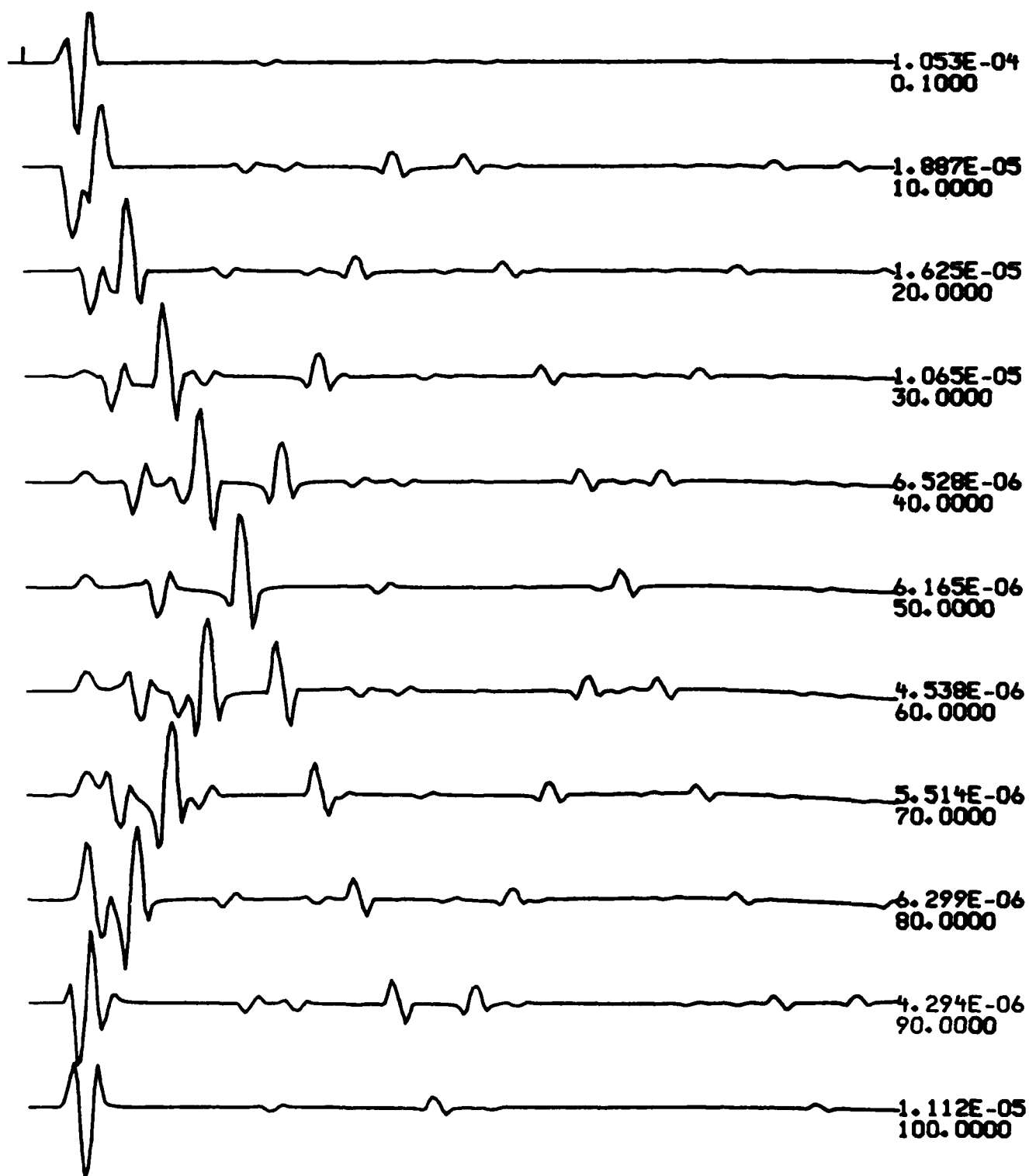


Fig. 1. Synthetic seismograms for the RDS component, using $\alpha=0.0039$ and $L=100\text{km}$.

R-T JSRC=4 RELATIVE AMPLITUDE



7 Fig. 2. Synthetic seismograms for the RDS component, using $\alpha=0.03125$ and $L=100\text{km}$.

R-T JSRC=4 RELATIVE AMPLITUDE

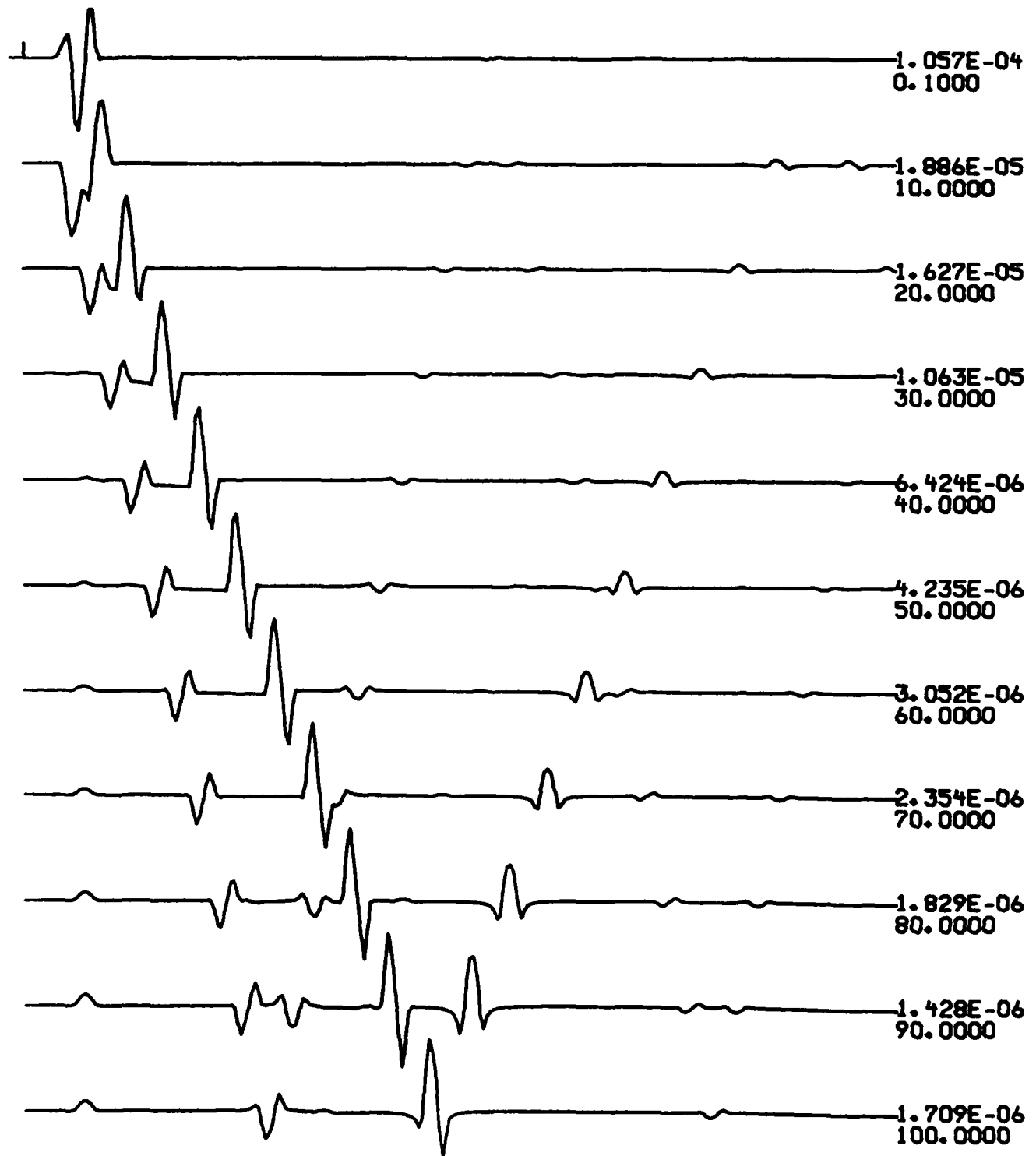


Fig. 3. Synthetic seismograms for the RDS component, using $\alpha=0.03125$ and $L=200\text{km}$.

R-T JSRC=4 RELATIVE AMPLITUDE

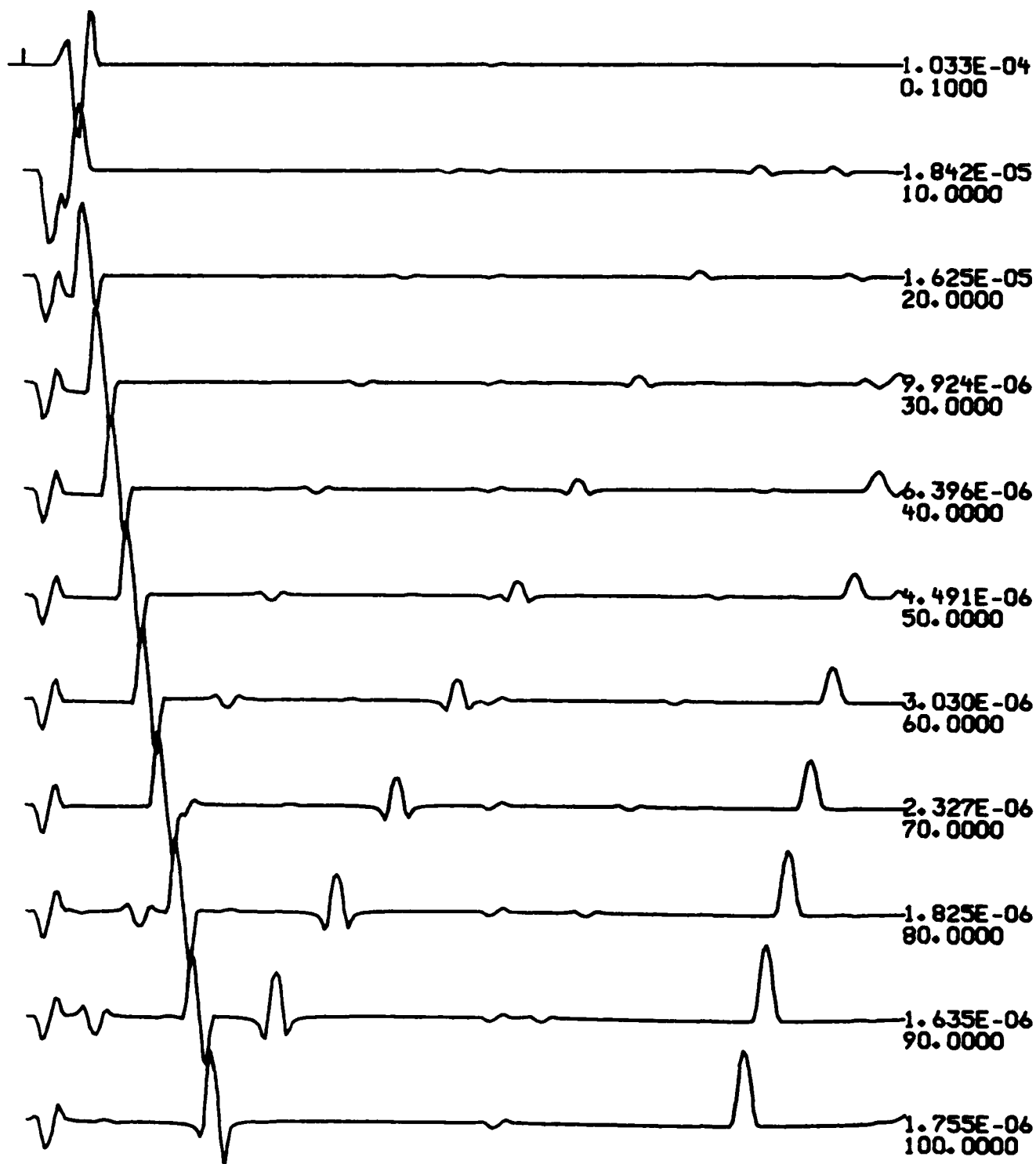


Fig. 4. Synthetic seismograms for the RDS component, using $\alpha=0.03125$ and $L=200\text{km}$, but using a reduced travel time display.

R-T JSRC=4 RELATIVE AMPLITUDE

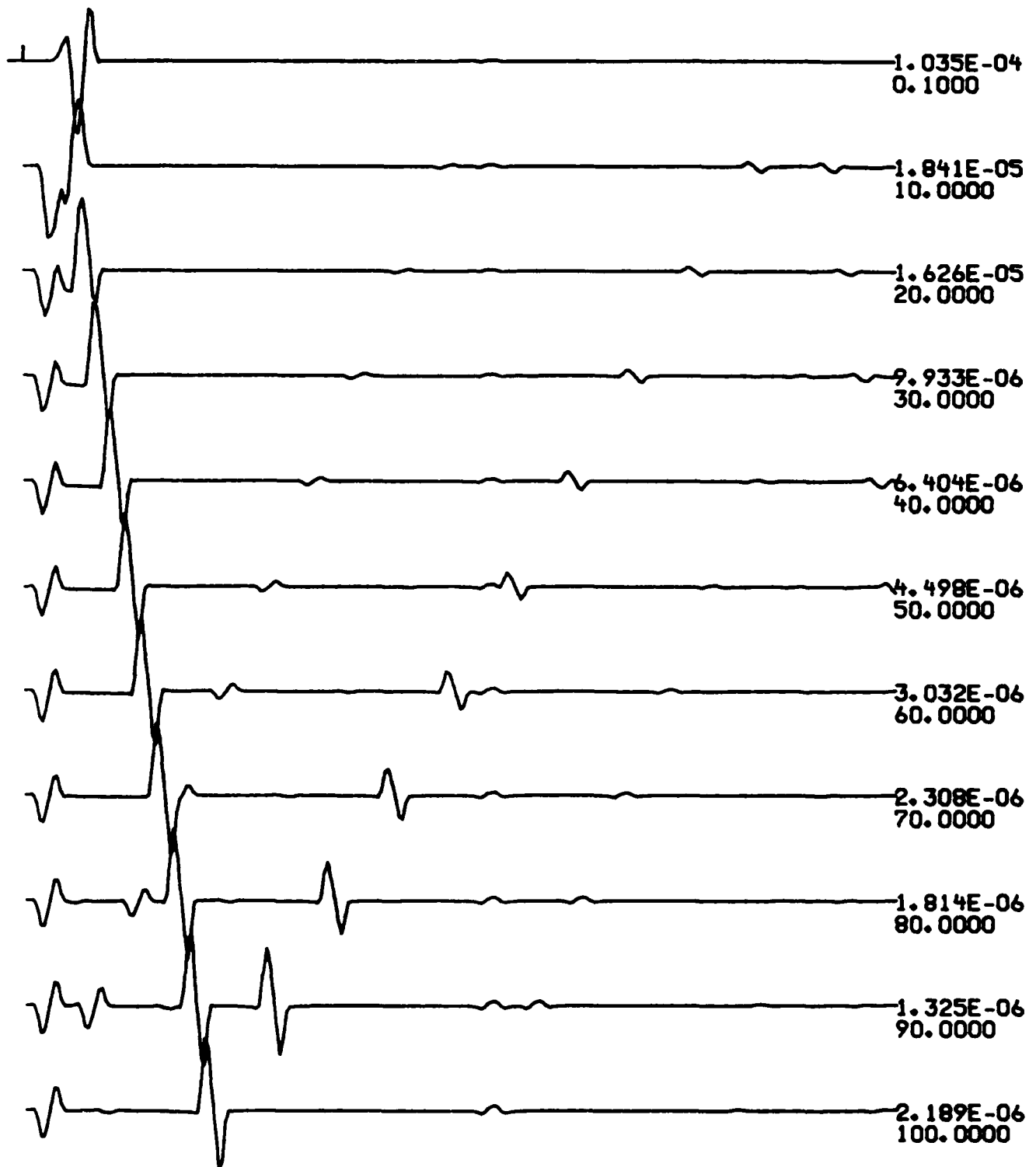


Fig. 5. Synthetic seismograms for the RDS component, using $\alpha=0.03125$ and $L=-200\text{km}$, a reduced travel time display, but using the shifted rectangular integration rule rather than the Bouchon trapezoidal integration rule.

R-T JSRC=4 RELATIVE AMPLITUDE

The following figures provide the ten Green's functions for the analytic solution, "whom," listed at the bottom of the model page, for the Bouchon integration scheme "W1000T0.00000," and for the modified rectangular rule, "W1000T0.21739."

Note that the modified rectangular rule does reduce the false $k = 0$ arrival. However, the synthetics obtained using the numerical integration techniques still have noise arrivals at large distances due to too small a choice for L . This noise is seen at distances larger than 300 km and corresponds to a P-wave arrival at a time of $(1000 - r)/6.15$ seconds. This is readily seen in the JSRC = 2, 9 or 10 Green's functions. There is no such problem with S arrivals, as seen in the predominantly SH Green's functions JSRC = 5 and 8.

ALPHA=0.047

DEPTH=10.000

FL =0.000

FU =2.000

DT =0.250

N, N1, N2:256,1,129

D	A	B	RHO	QA INV	QB INV
11.000	6.150	3.550	2.800	0.00010	0.00010
	6.150	3.550	2.800	0.00010	0.00010

ND = 11

DMIN=1.00000E+02

DD =0.00000E+00

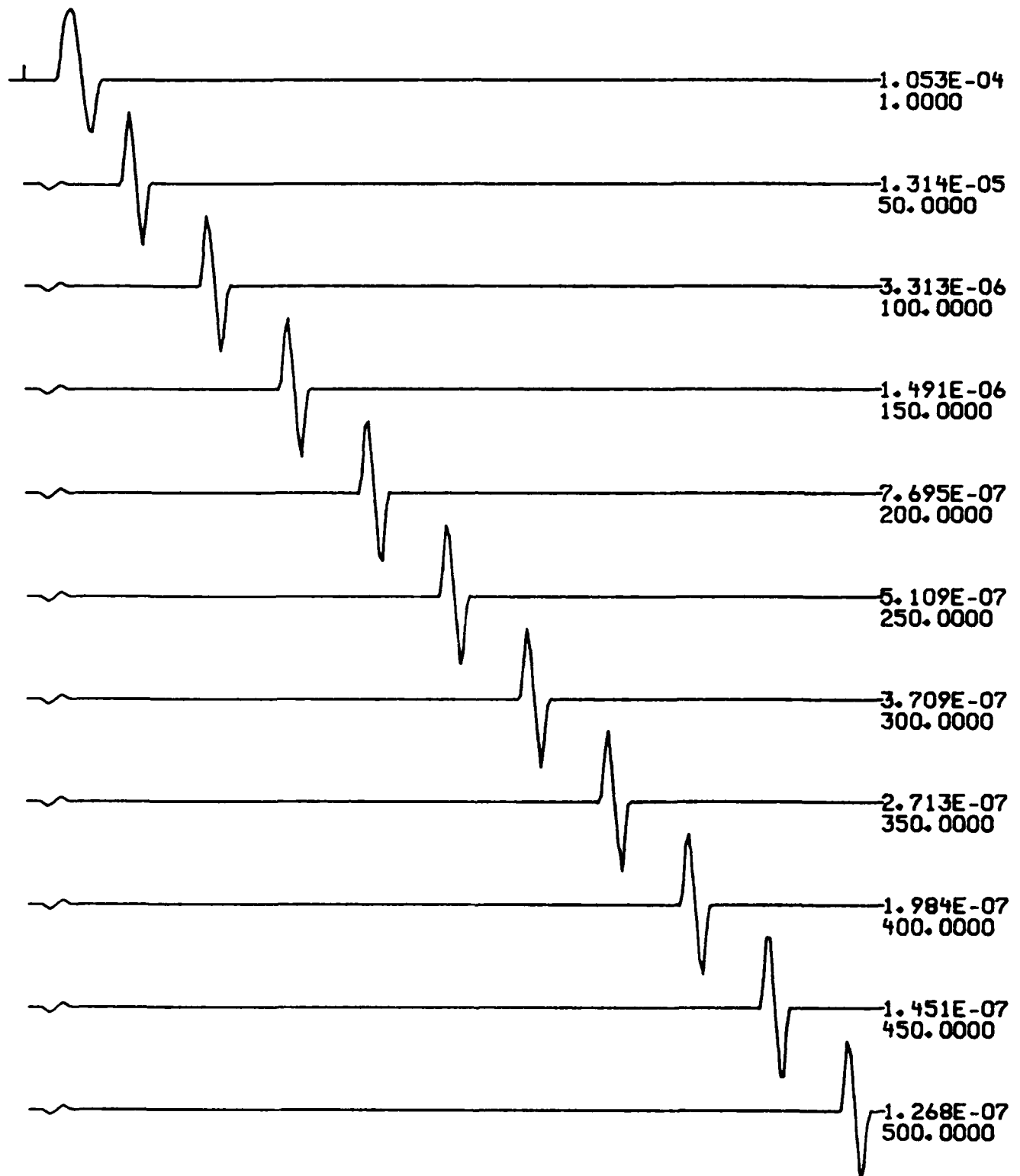
TMIN =0.0000

TMAX =63.75000

(R,T)

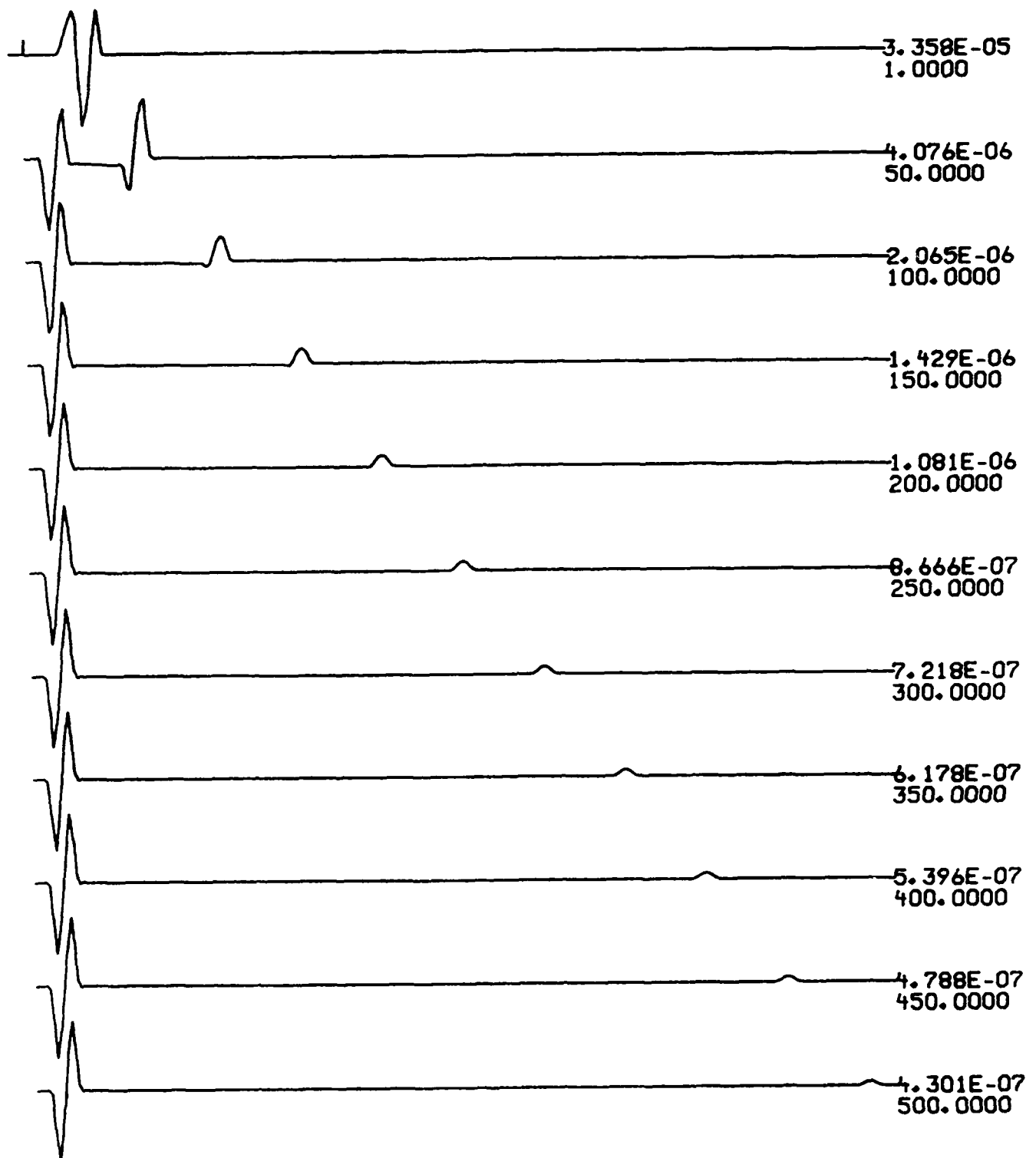
PARABOLIC ITYPE=4

whom

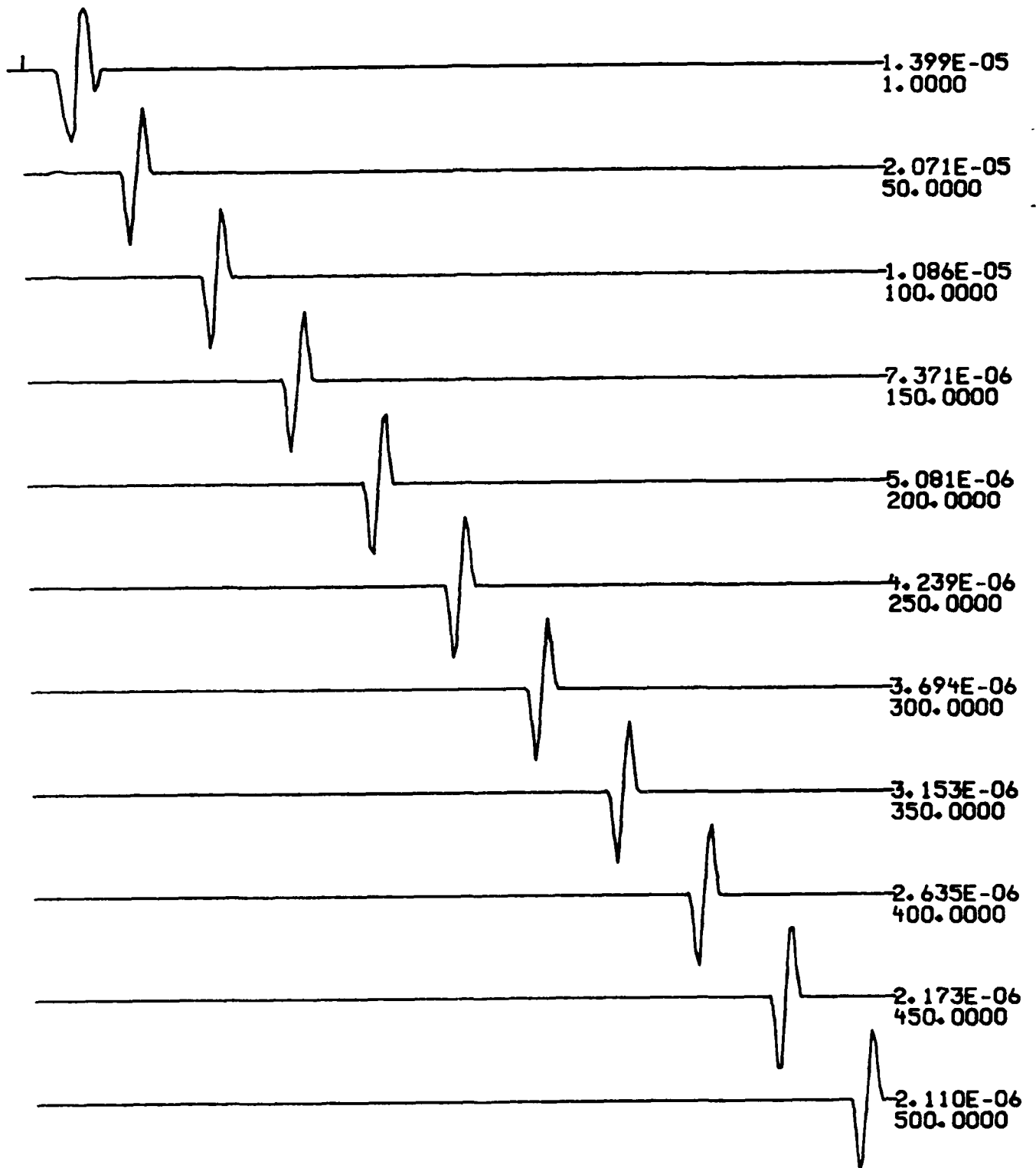


7

R-T JSRC=1 RELATIVE AMPLITUDE

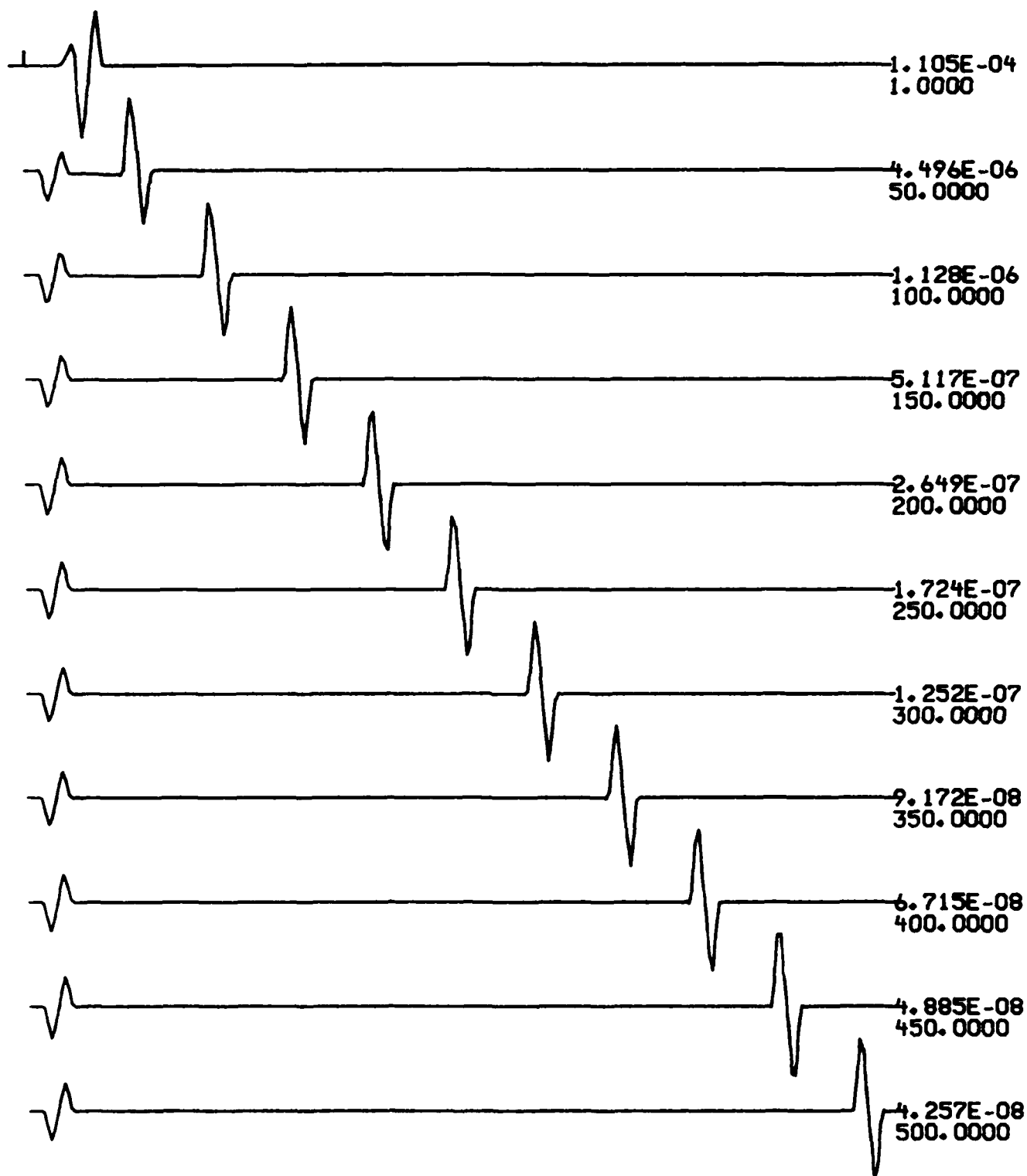


R-T JSRC=2 RELATIVE AMPLITUDE



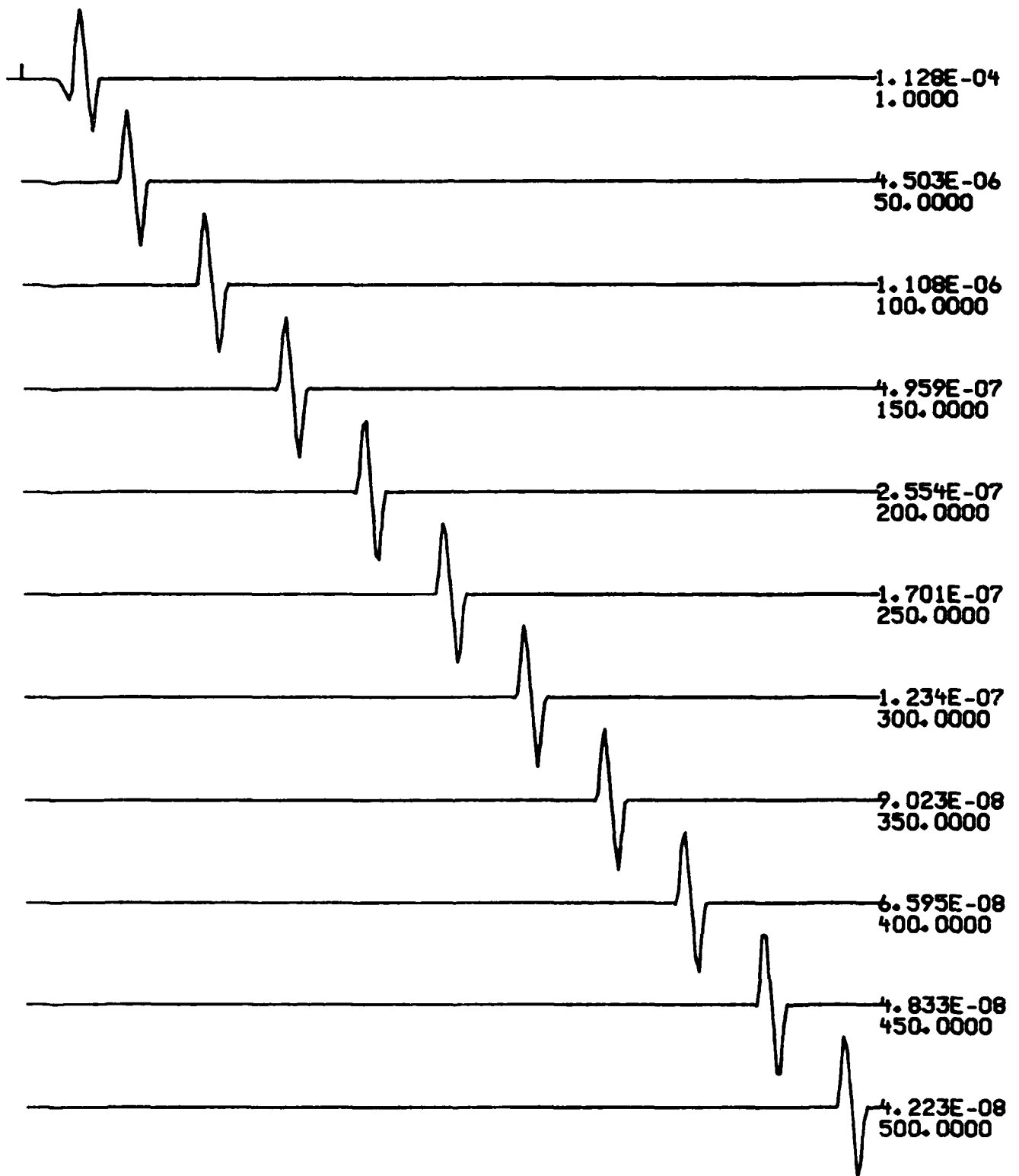
7

R-T JSRC=3 RELATIVE AMPLITUDE



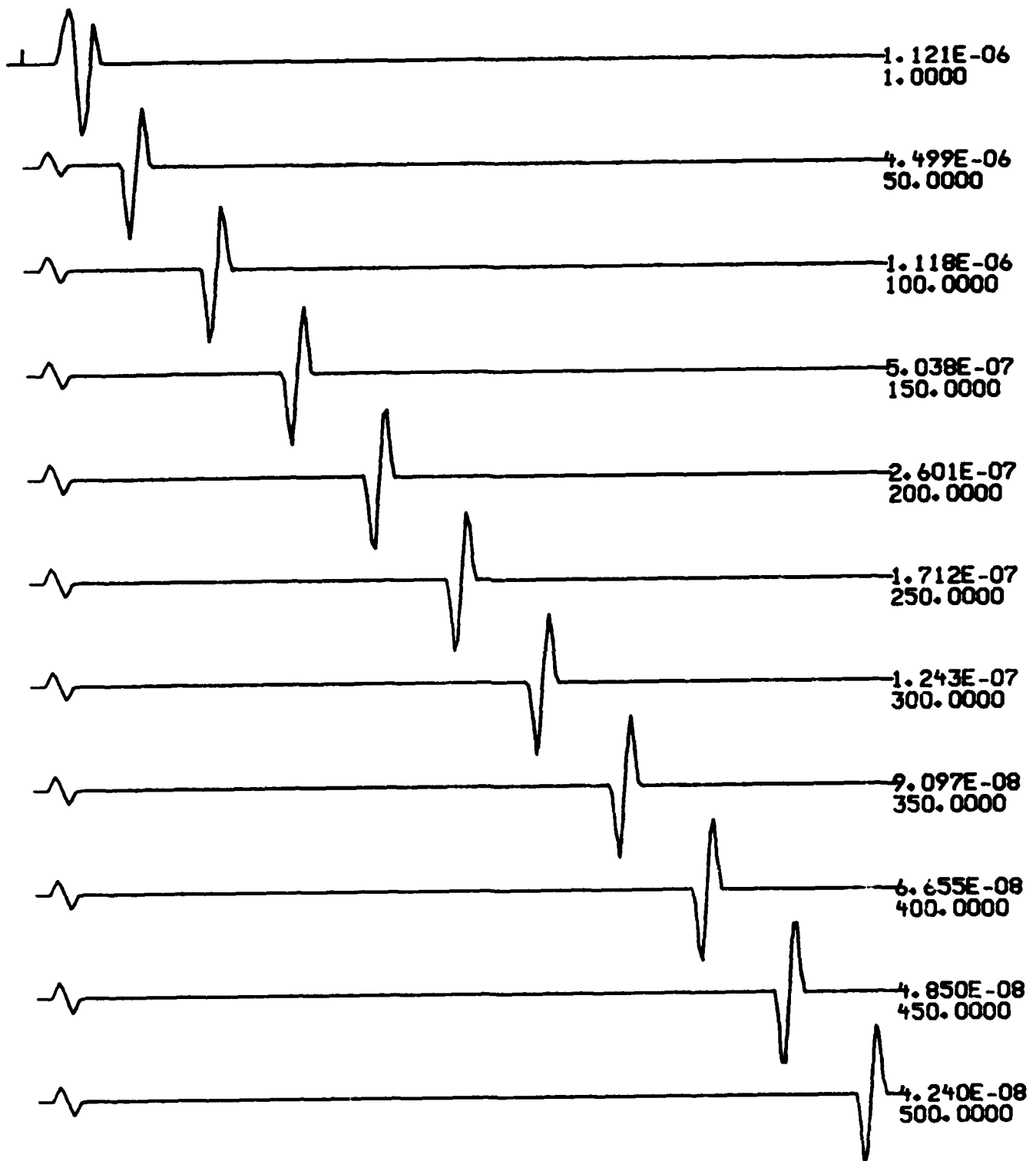
7

R-T JSRC=4 RELATIVE AMPLITUDE

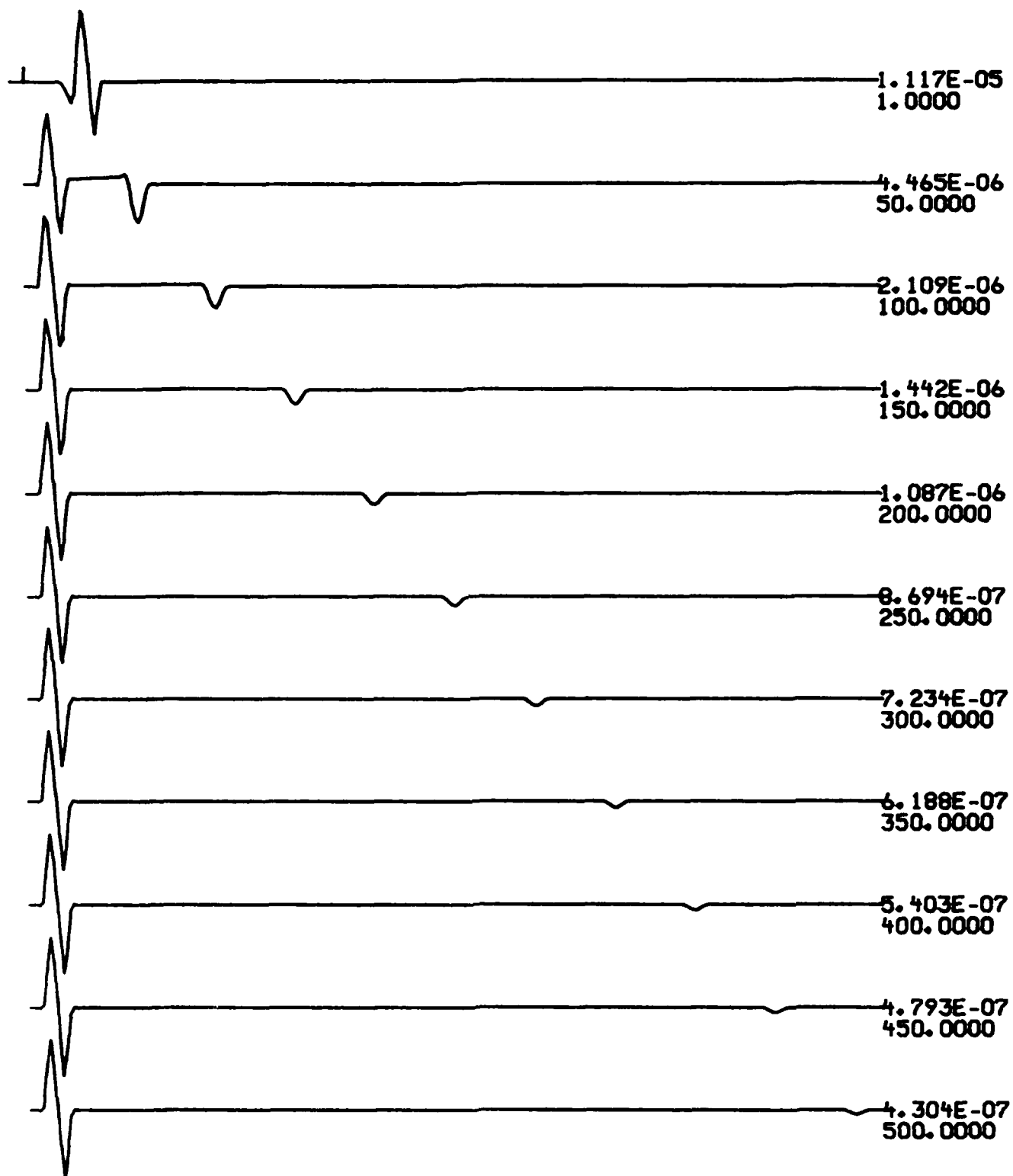


7

R-T JSRC=5 RELATIVE AMPLITUDE

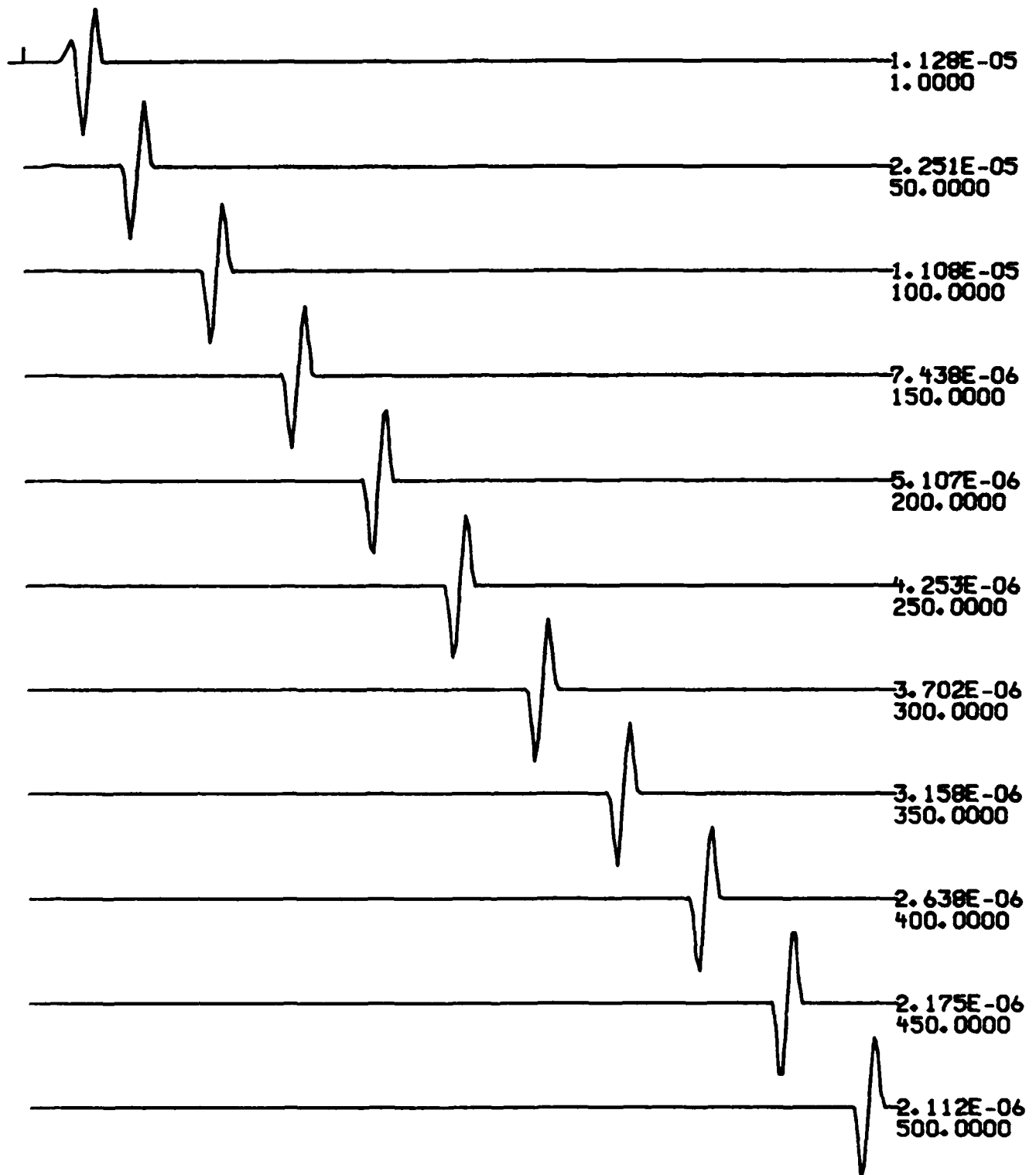


R-T JSRC=6 RELATIVE AMPLITUDE



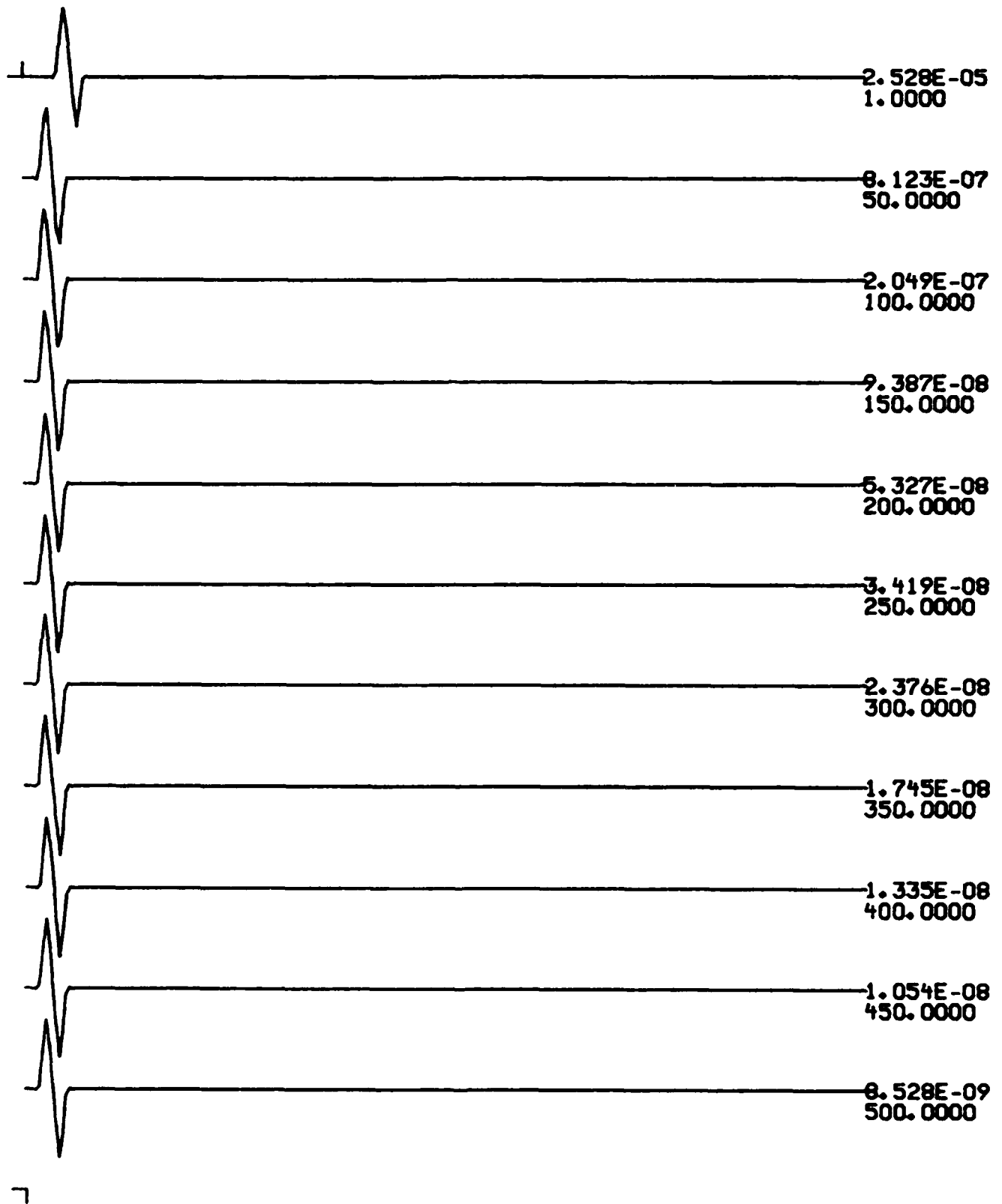
R-T

JSRC=7 RELATIVE AMPLITUDE



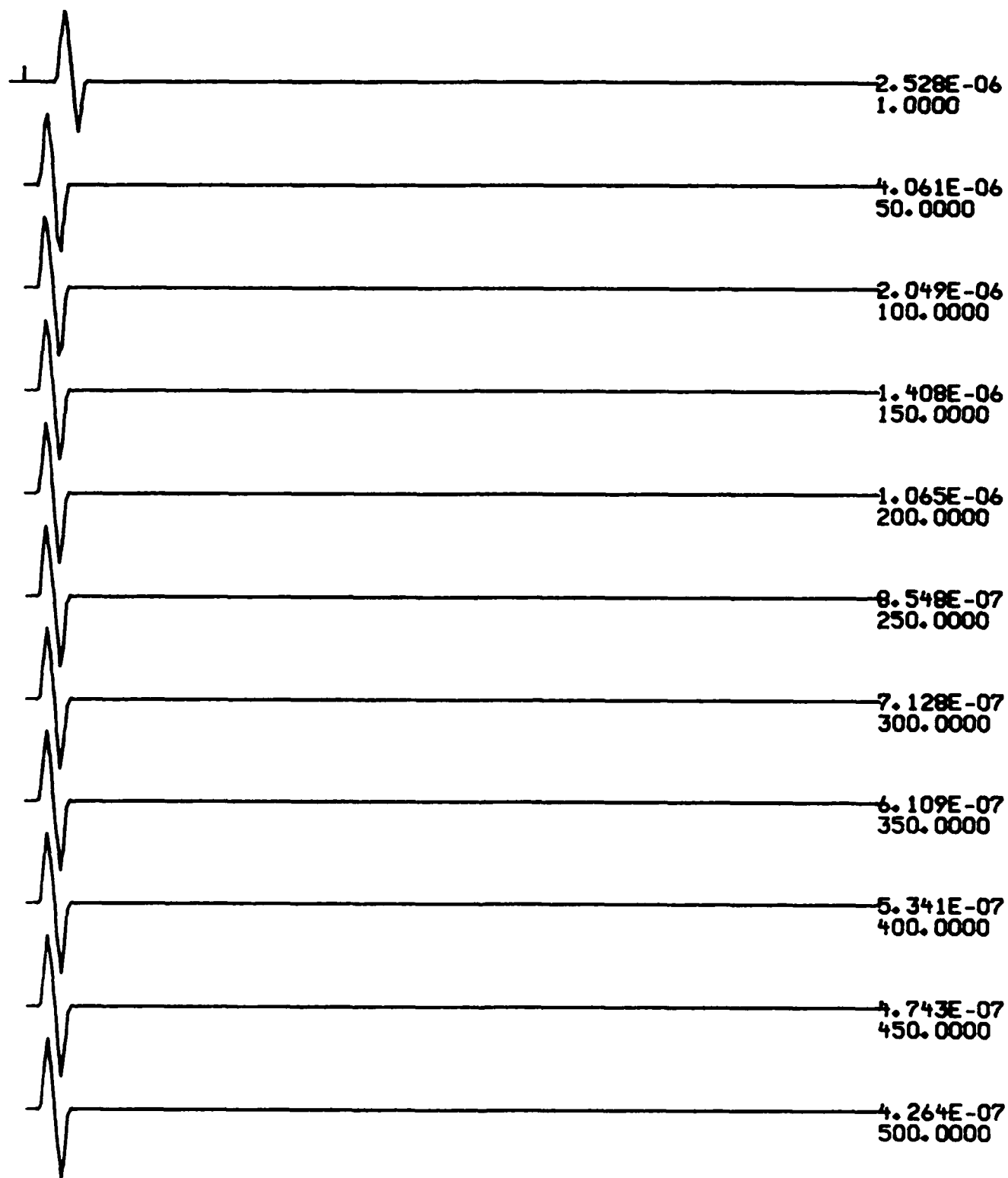
7

R-T JSRC=8 RELATIVE AMPLITUDE



7

R-T JSRC=9 RELATIVE AMPLITUDE



7

R-T

JSRC=10 RELATIVE AMPLITUDE

ALPHA=0.047

DEPTH=10.000

FL =0.000

FU =2.000

DT =0.250

N, N1, N2:256,1,129

D	A	B	RHO	QA INV	QB INV
---	---	---	-----	--------	--------

11.000	6.150	3.550	2.800	0.00010	0.00010
--------	-------	-------	-------	---------	---------

	6.150	3.550	2.800	0.00010	0.00010
--	-------	-------	-------	---------	---------

ND = 11

DMIN=1.00000E+02

DD =0.00000E+00

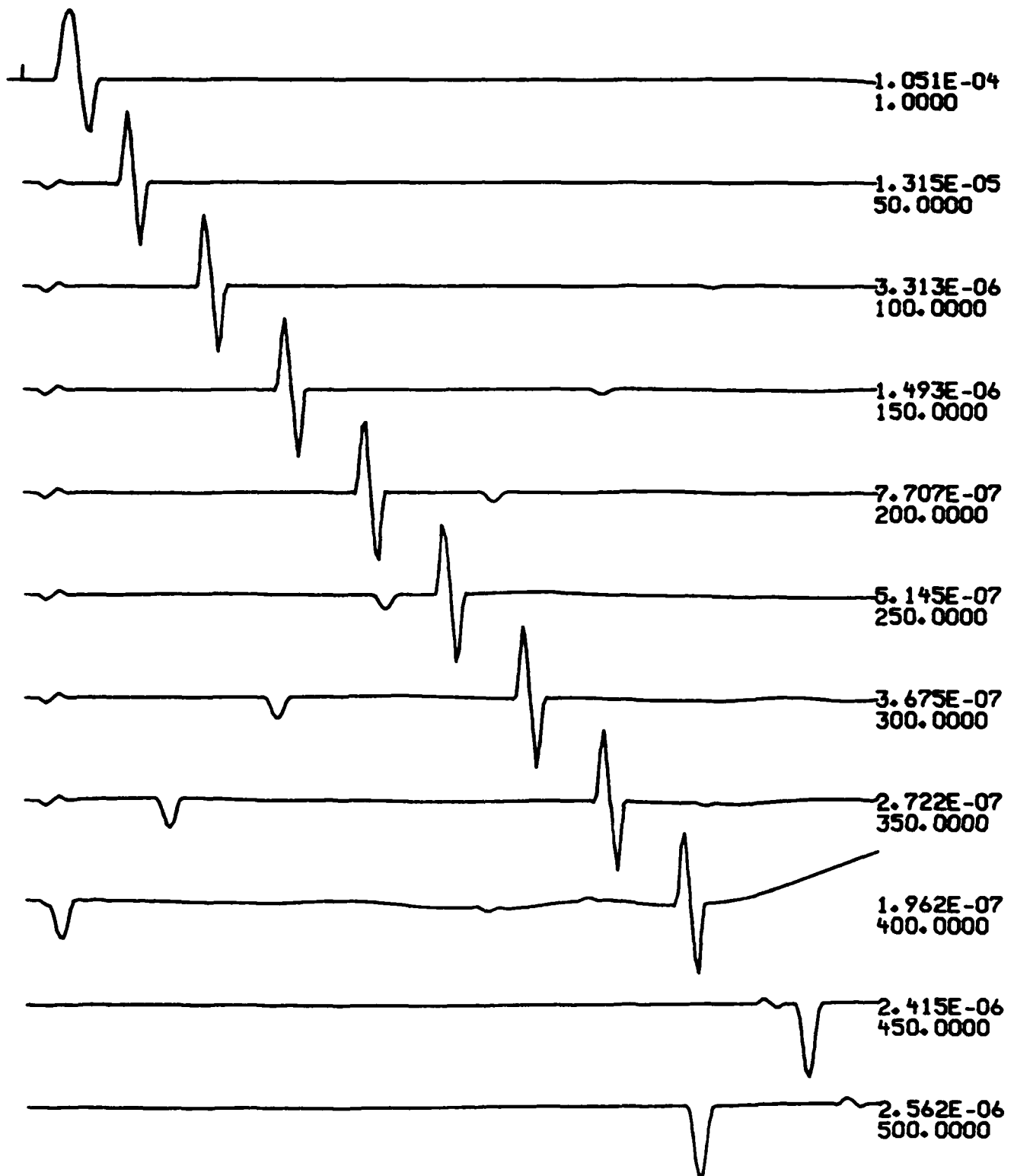
TMIN =0.0000

TMAX =63.75000

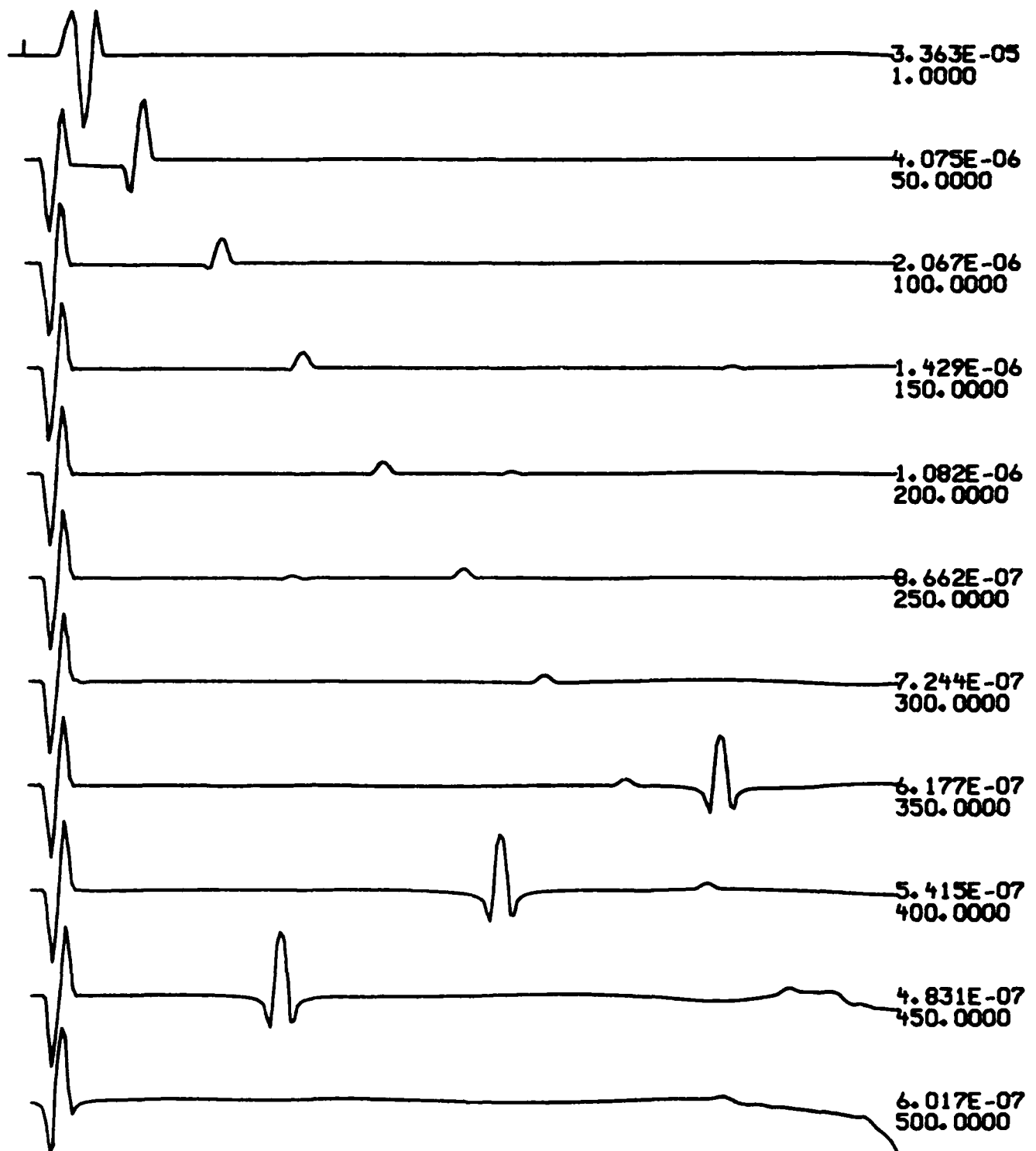
(R,T)

PARABOLIC ITYPE=4

W1000T0.00000

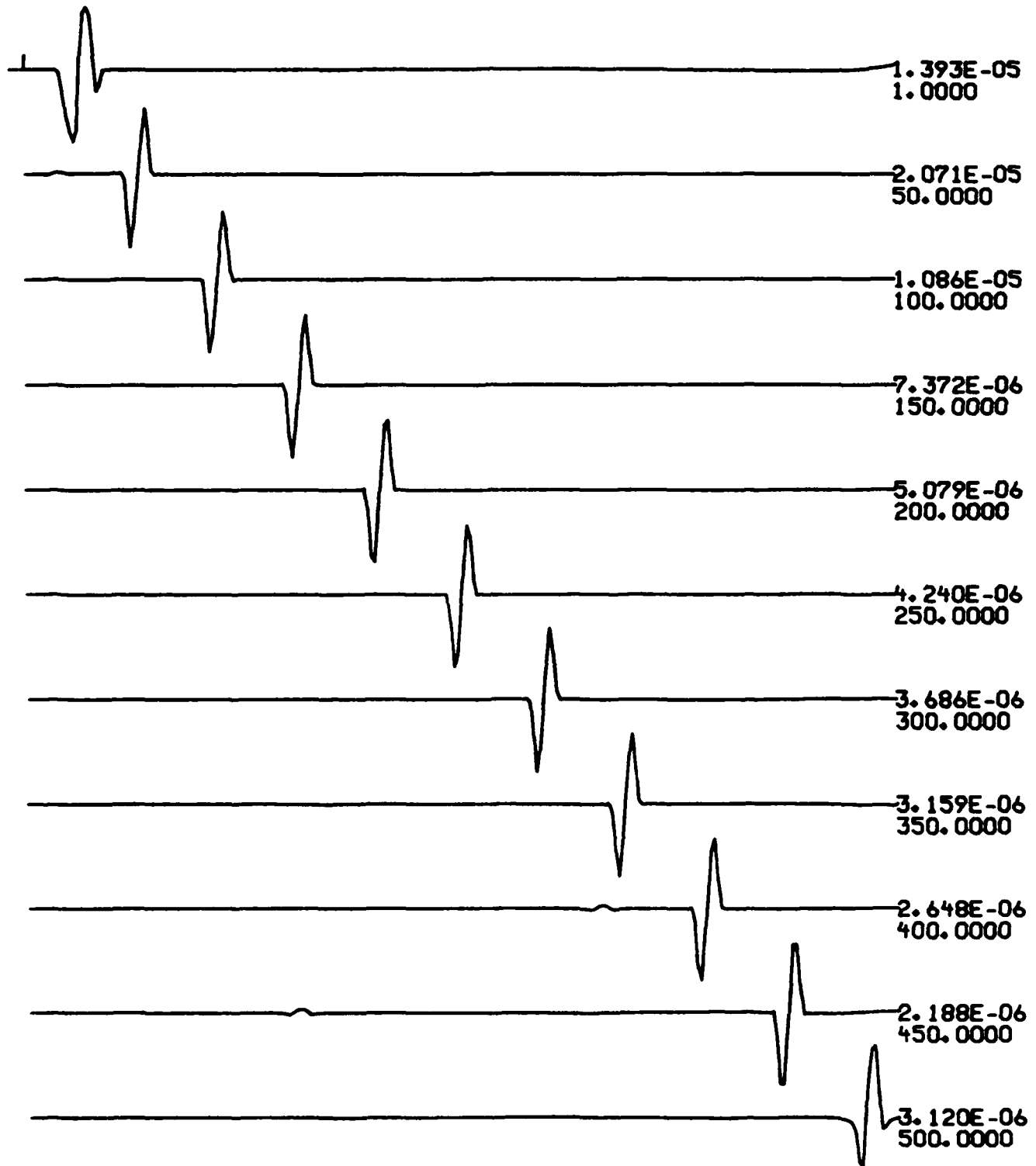


R-T JSRC=1 RELATIVE AMPLITUDE



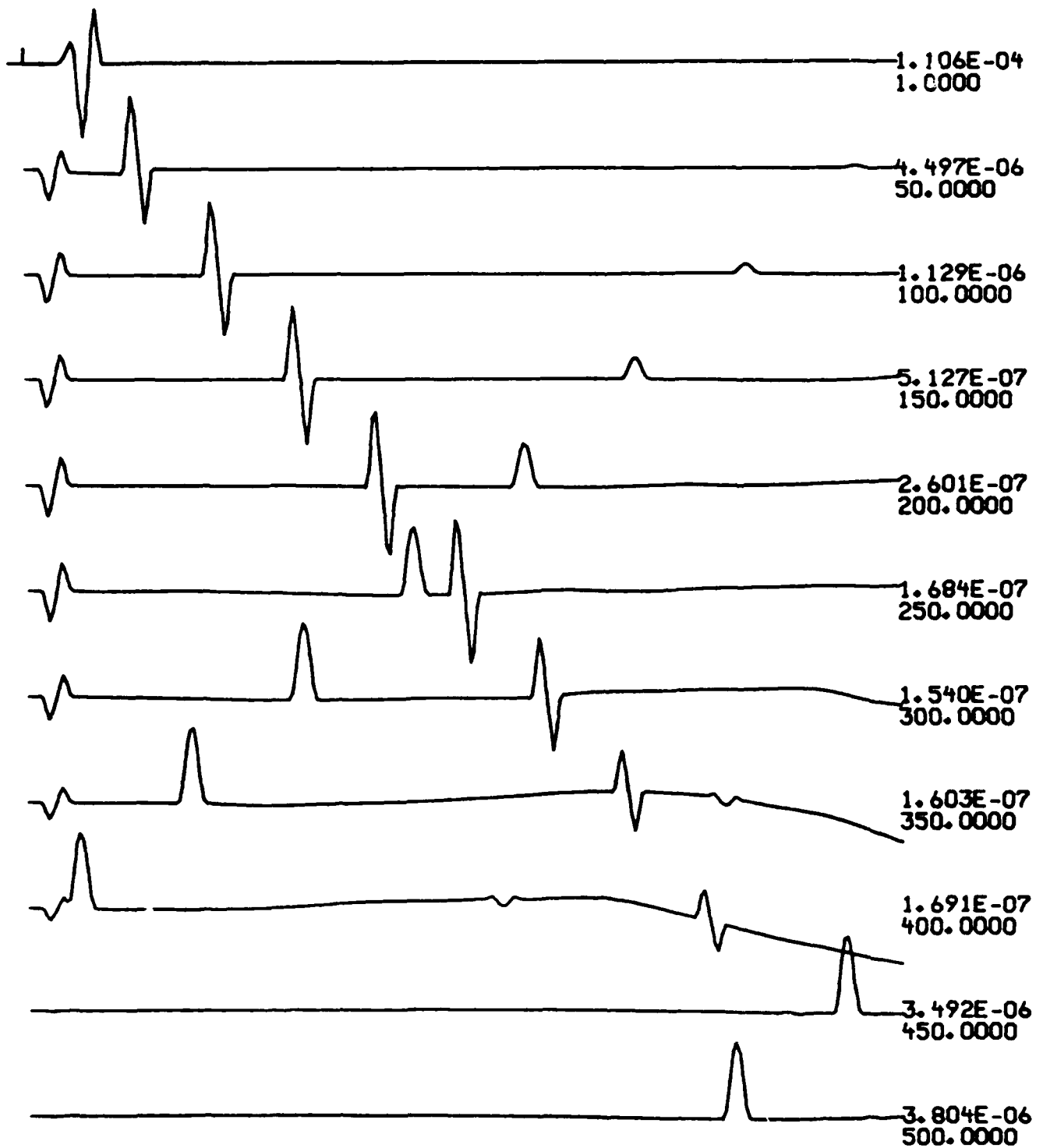
7

R-T JSRC=2 RELATIVE AMPLITUDE



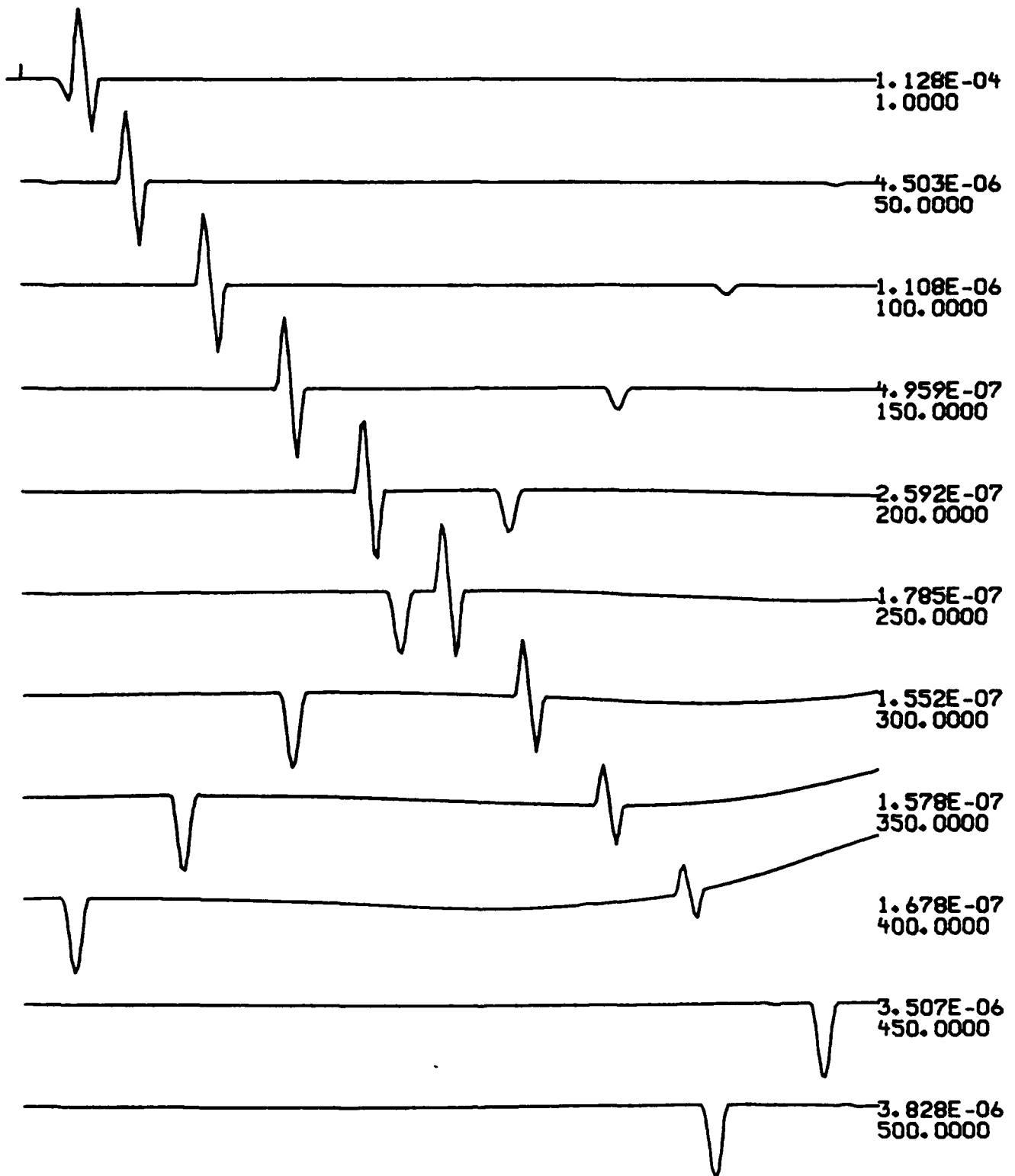
7

R-T JSRC=3 RELATIVE AMPLITUDE



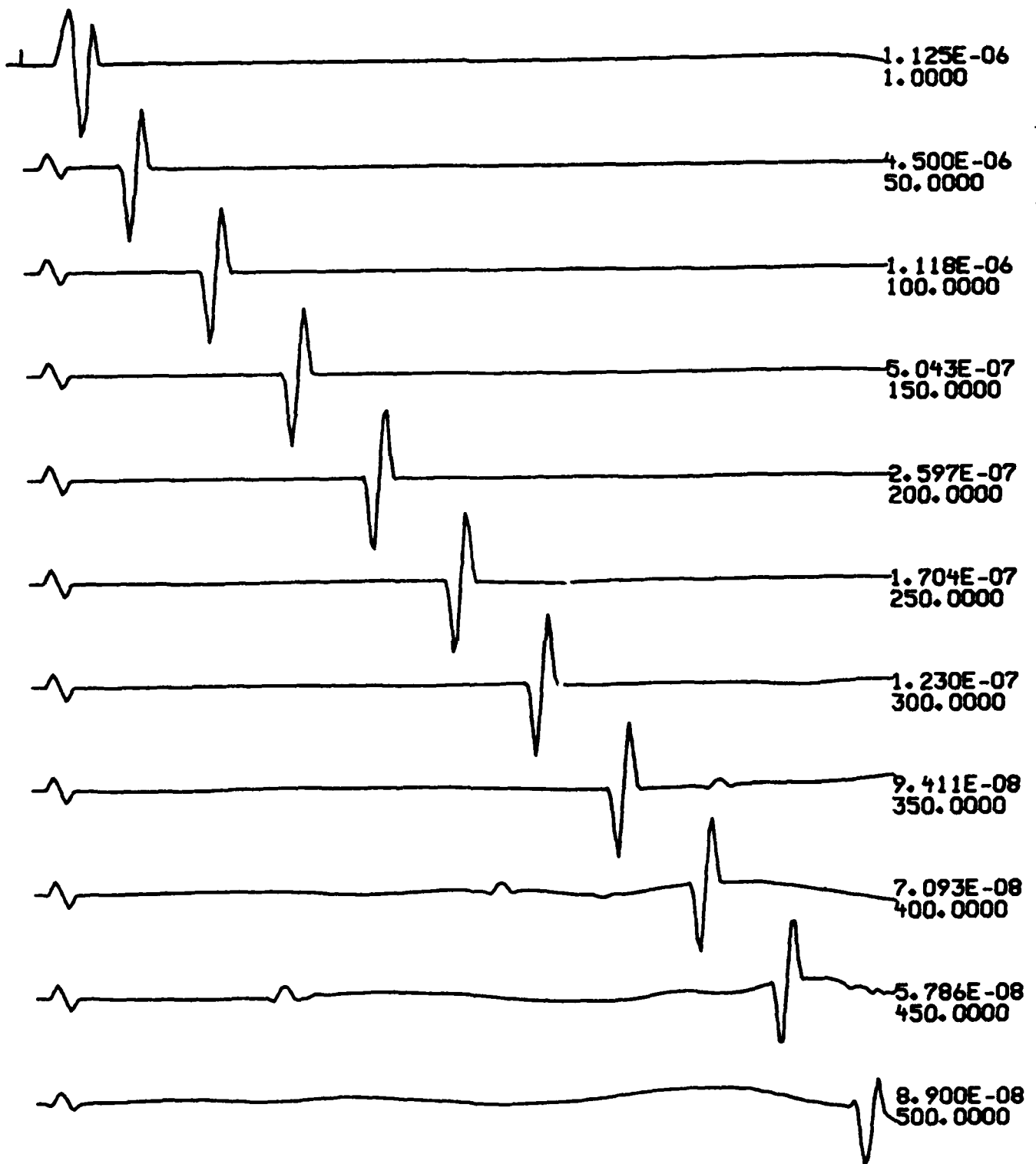
7

R-T JSRC=4 RELATIVE AMPLITUDE



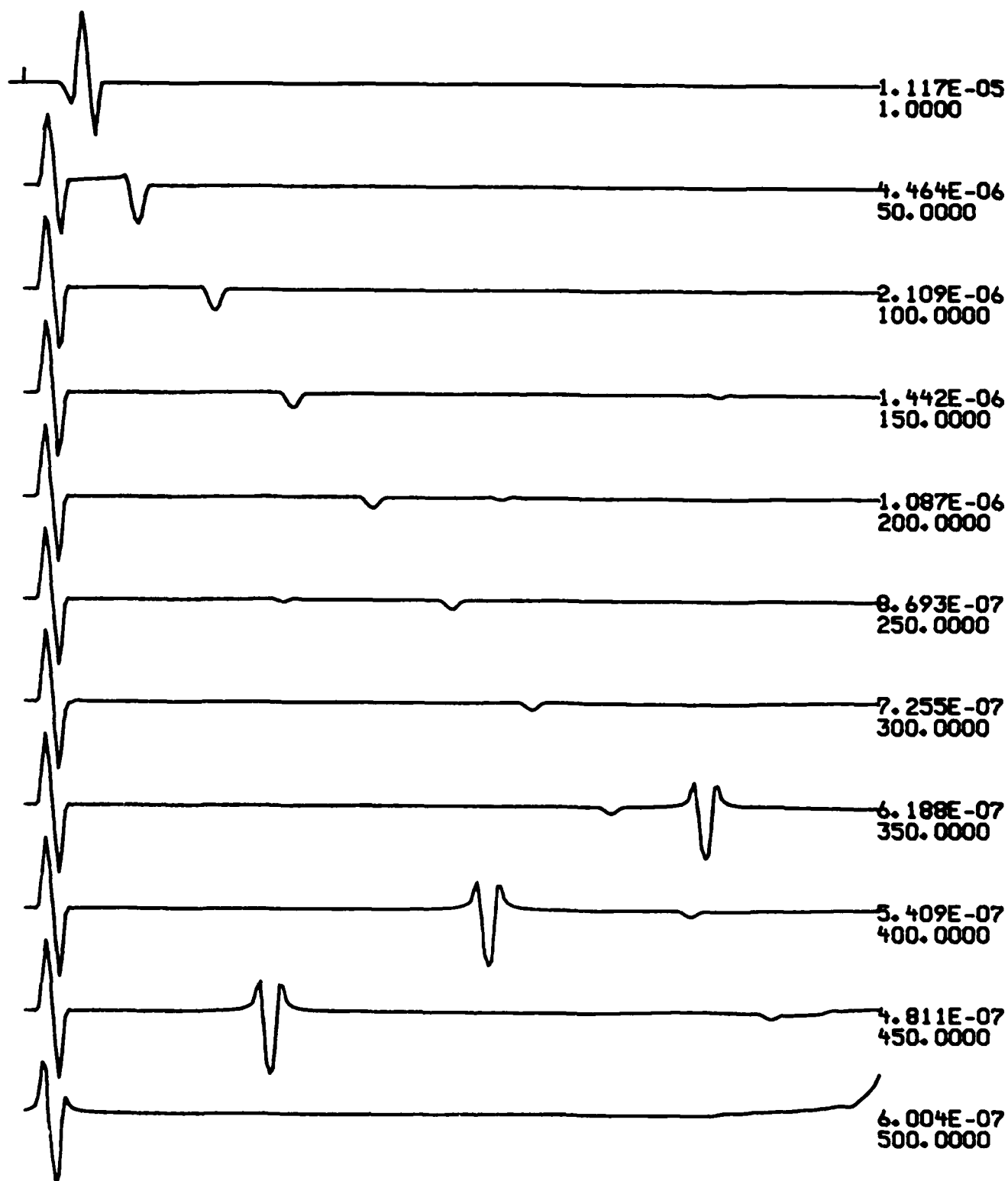
7

R-T JSRC=5 RELATIVE AMPLITUDE

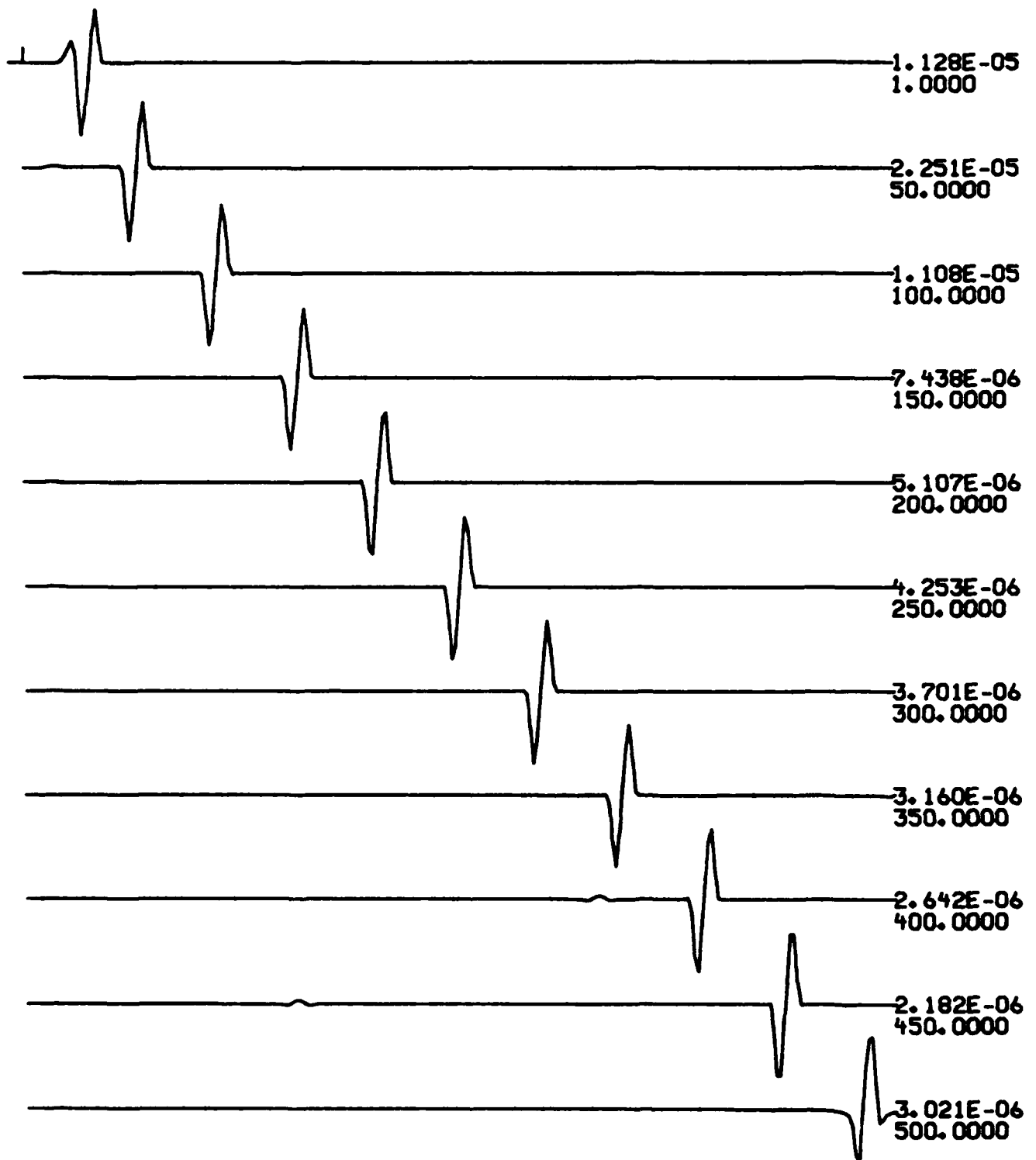


7

R-T JSRC=6 RELATIVE AMPLITUDE

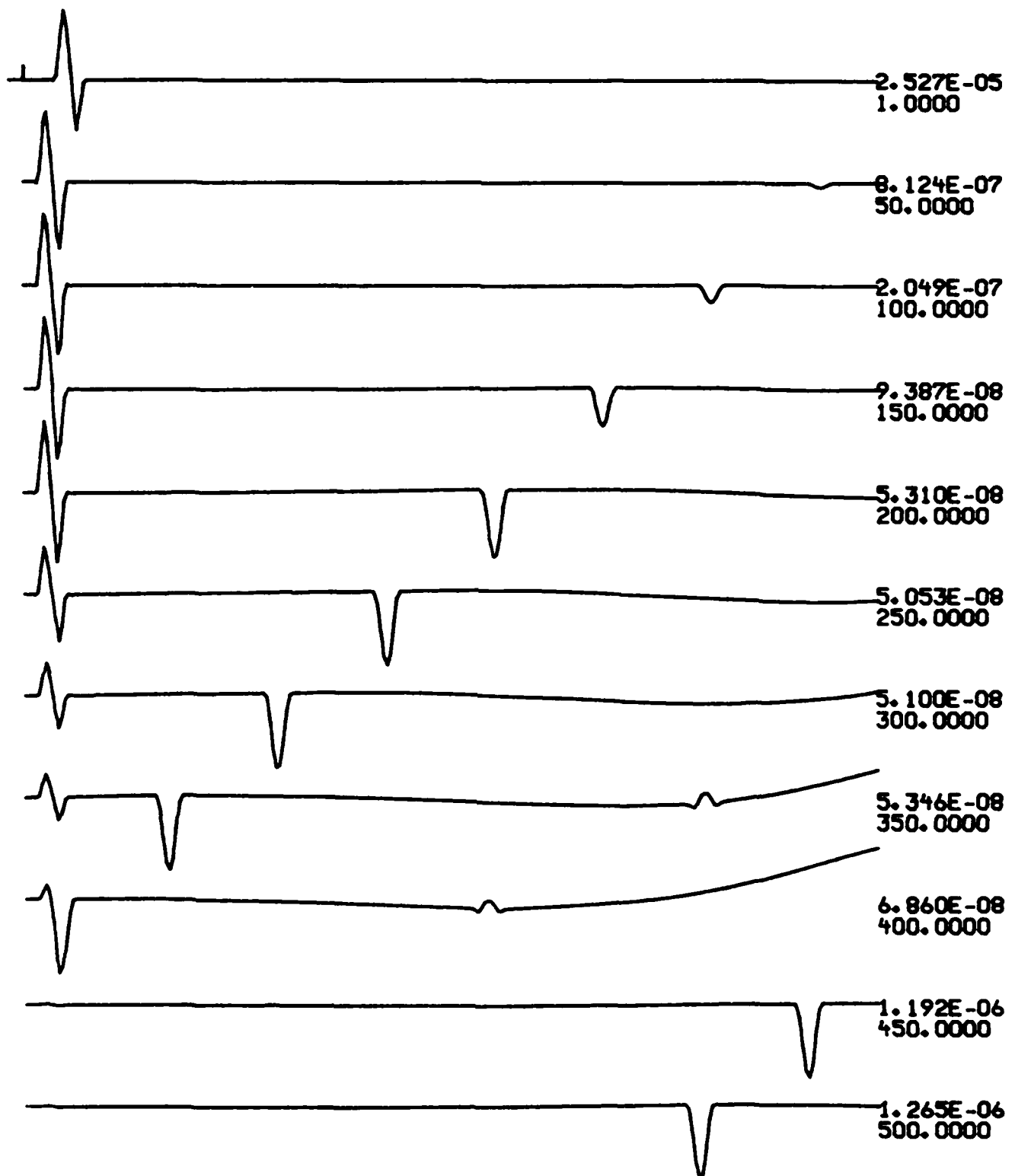


R-T JSRC=7 RELATIVE AMPLITUDE



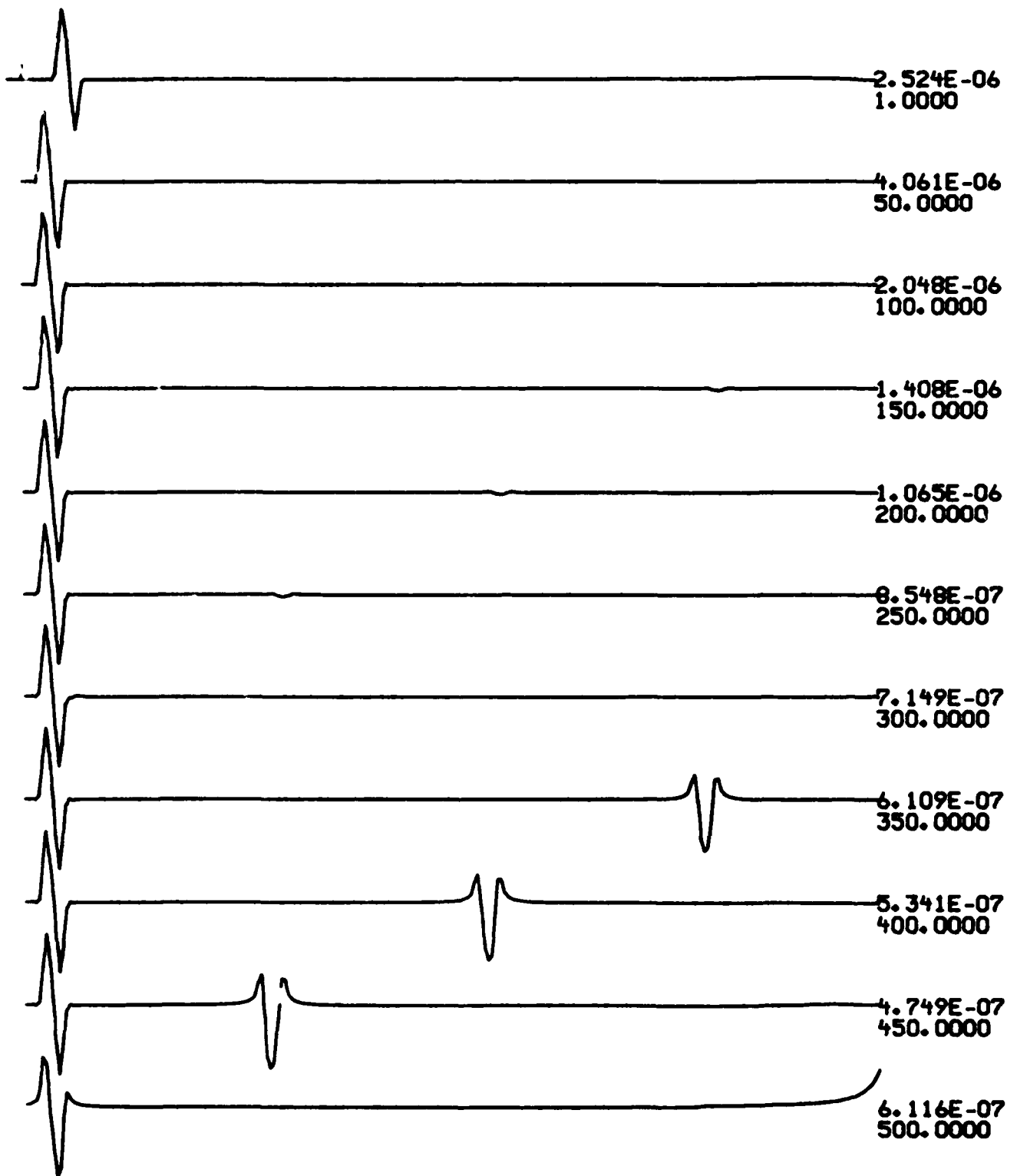
7

R-T JSRC=8 RELATIVE AMPLITUDE



7

R-T JSRC=9 RELATIVE AMPLITUDE



7

R-T JSRC=10 RELATIVE AMPLITUDE

ALPHA=0.047

DEPTH=10.000

FL =0.000

FU =2.000

DT =0.250

N, N1, N2:256,1,129

D	A	B	RHO	QA INV	QB INV
11.000	6.150	3.550	2.800	0.00010	0.00010
	6.150	3.550	2.800	0.00010	0.00010

ND = 11

DMIN=1.00000E+02

DD =0.00000E+00

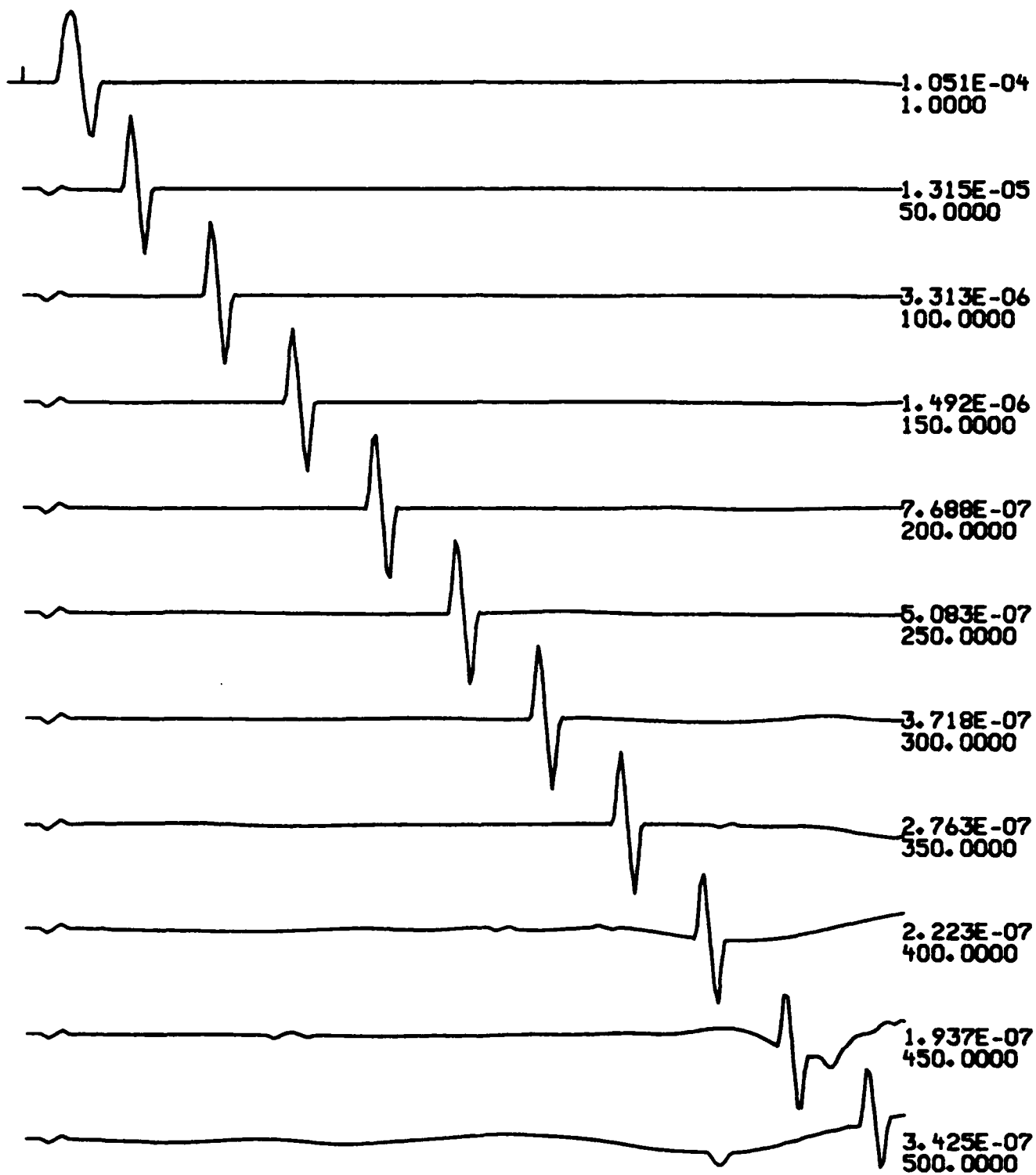
TMIN =0.0000

TMAX =63.75000

(R,T)

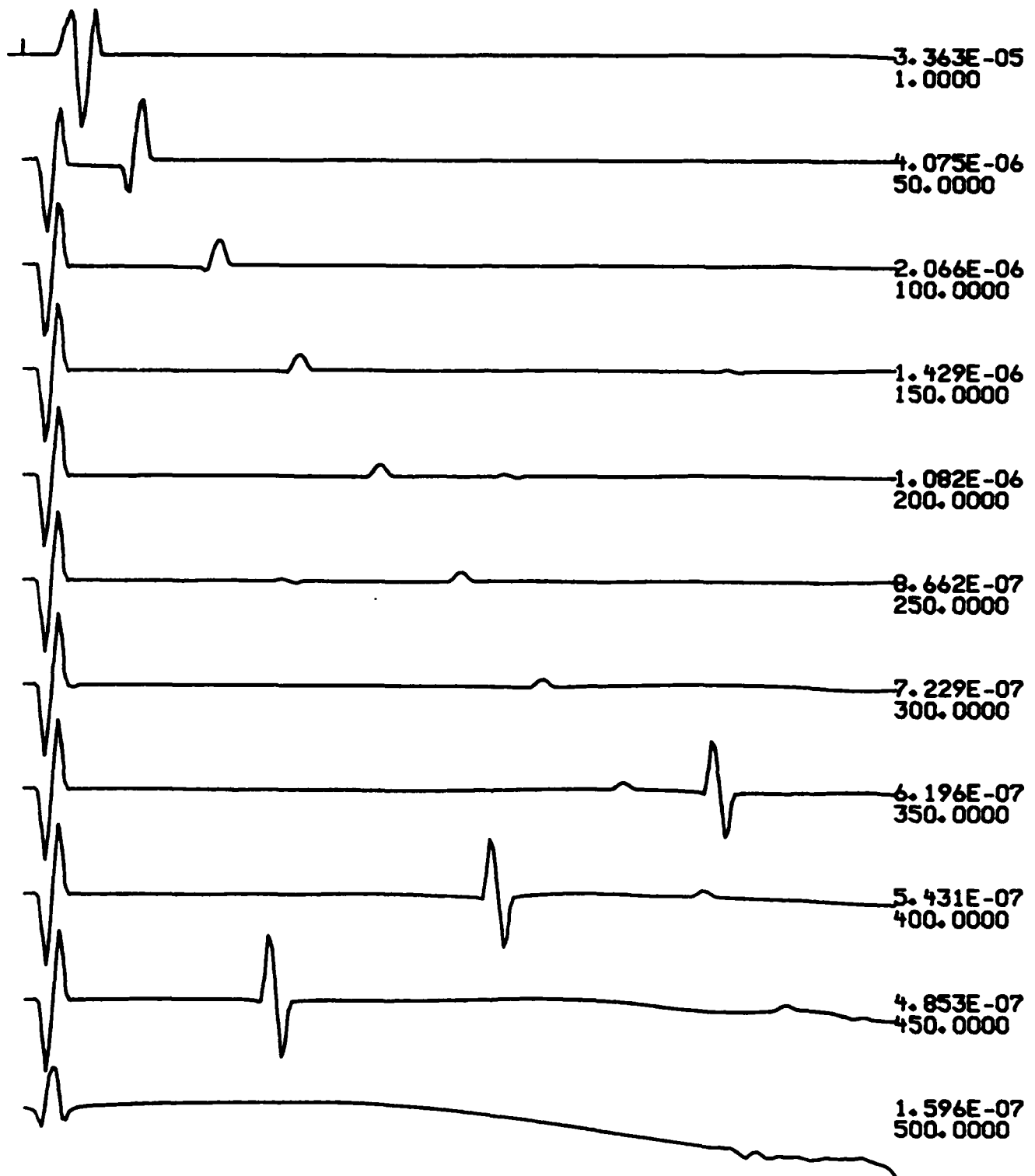
PARABOLIC ITYPE=4

W1000T0.21739



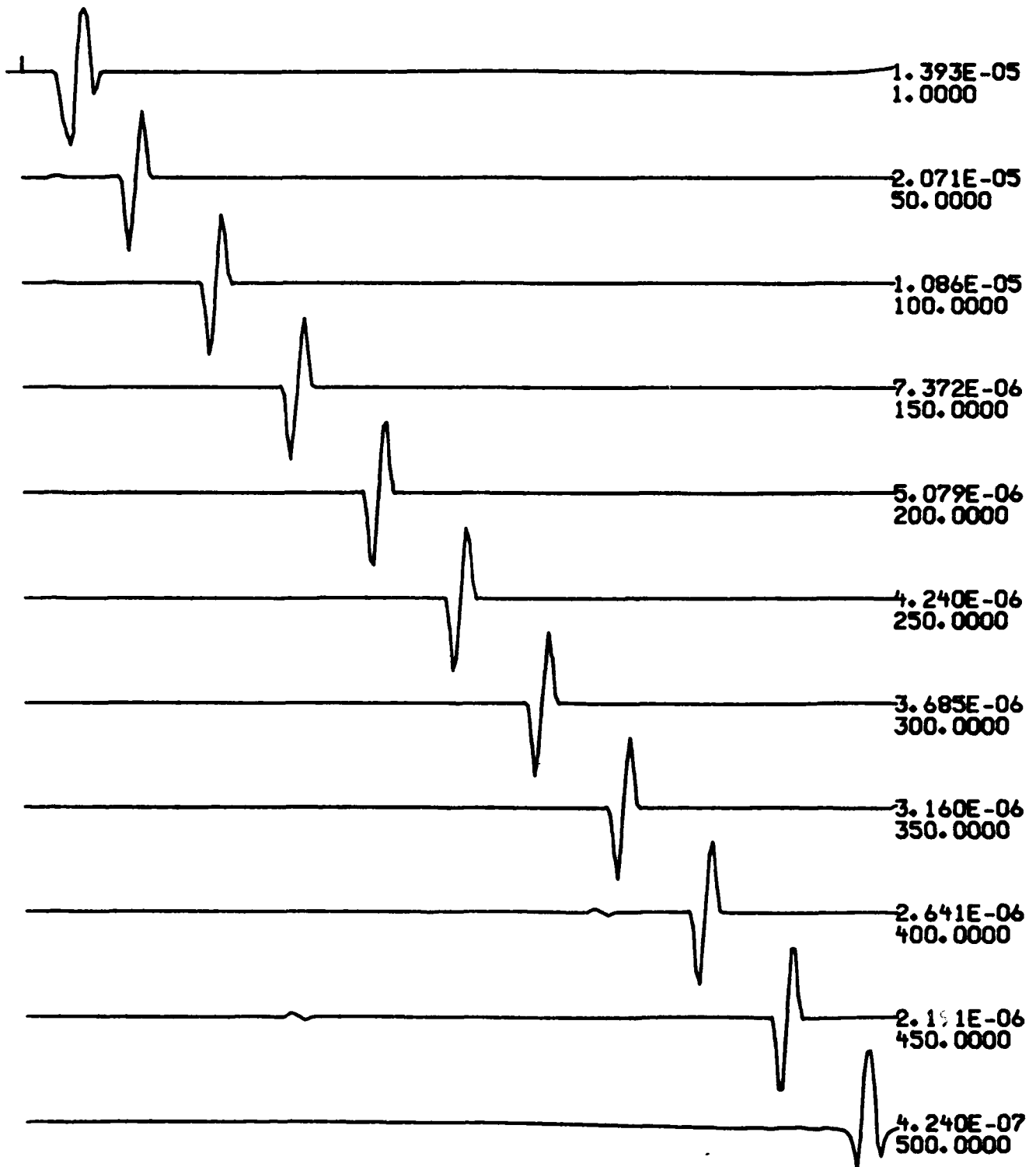
7

R-T JSRC=1 RELATIVE AMPLITUDE



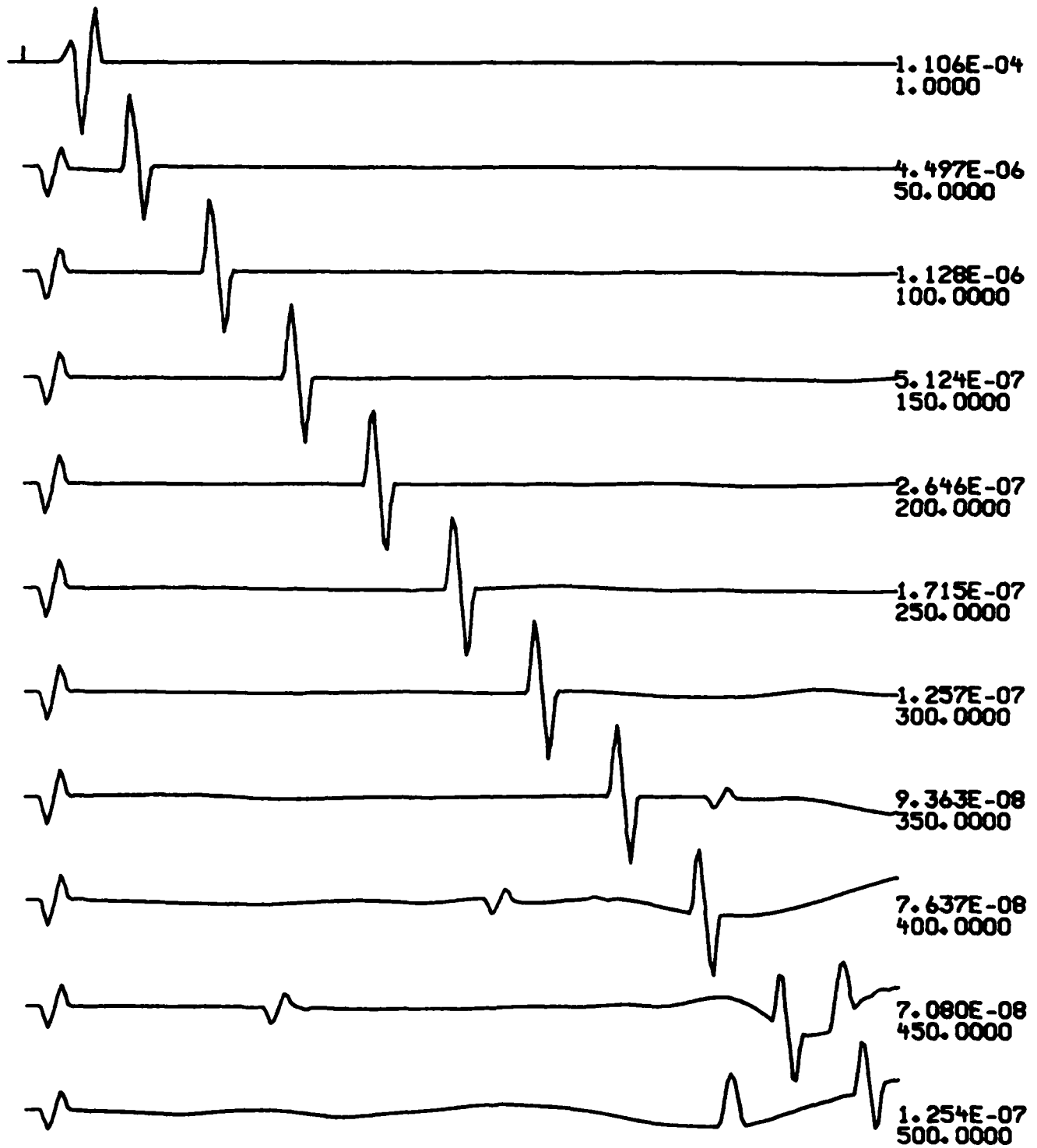
7

R-T JSRC=2 RELATIVE AMPLITUDE



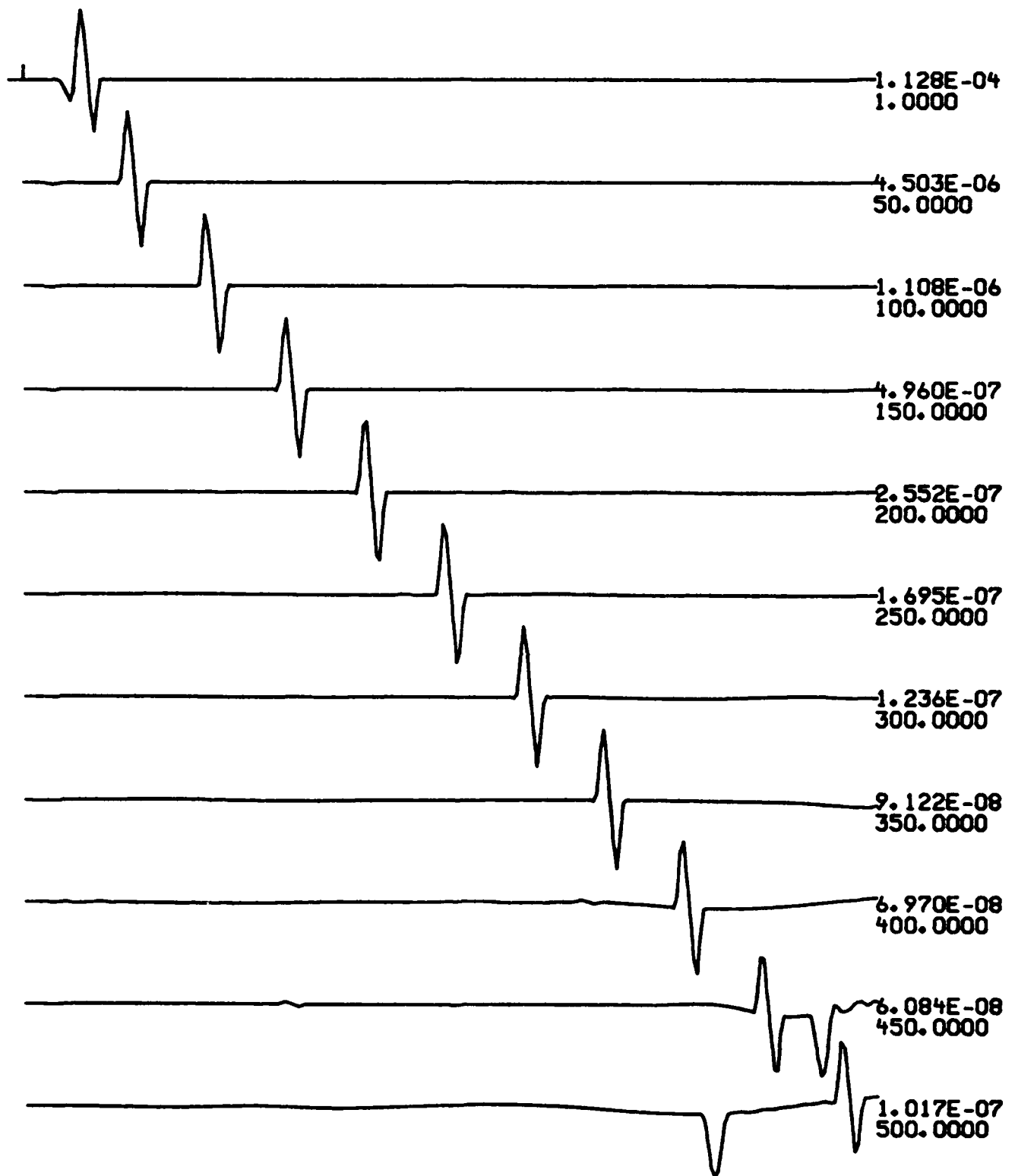
7

R-T JSRC=3 RELATIVE AMPLITUDE

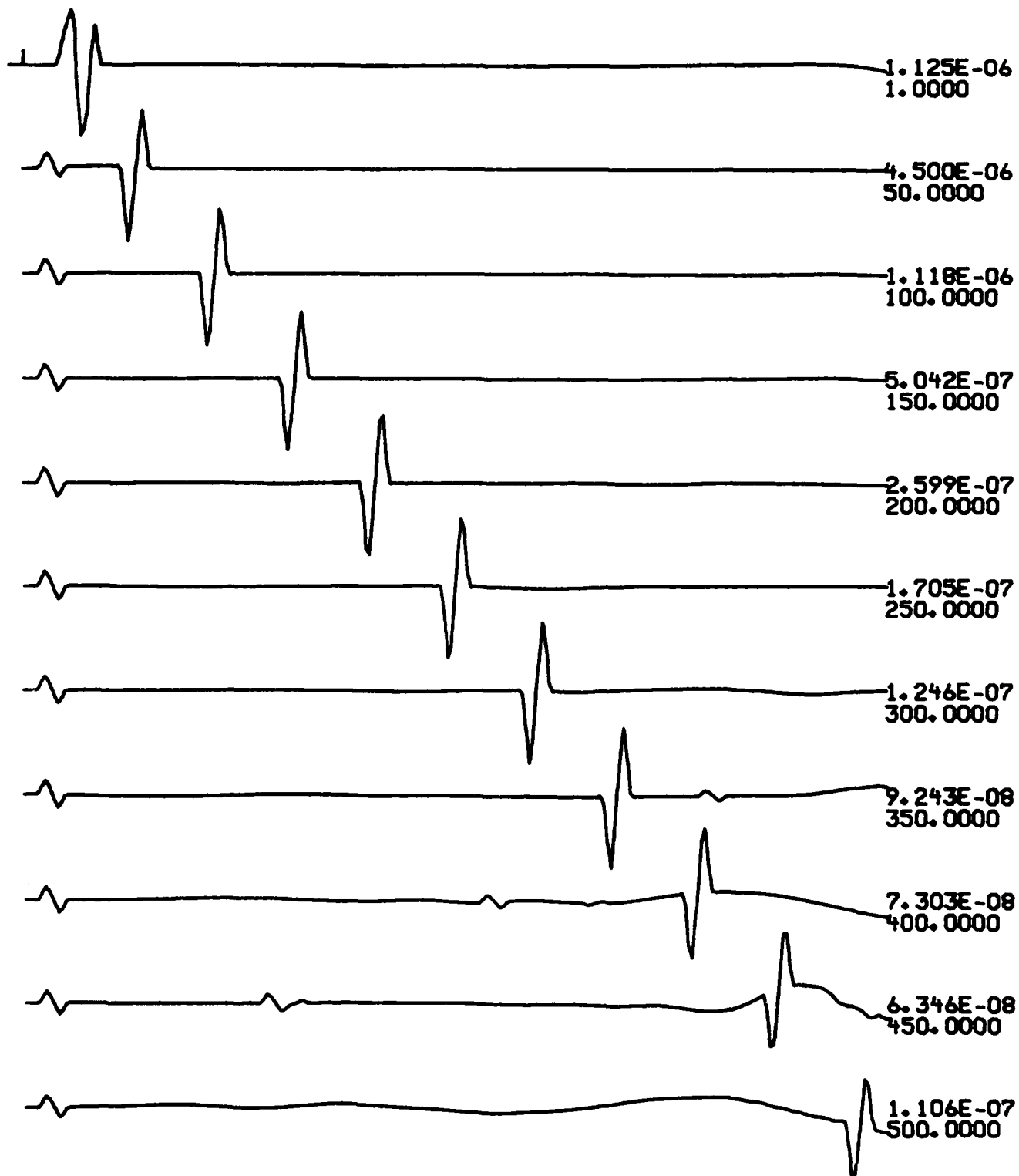


7

R-T JSRC=4 RELATIVE AMPLITUDE

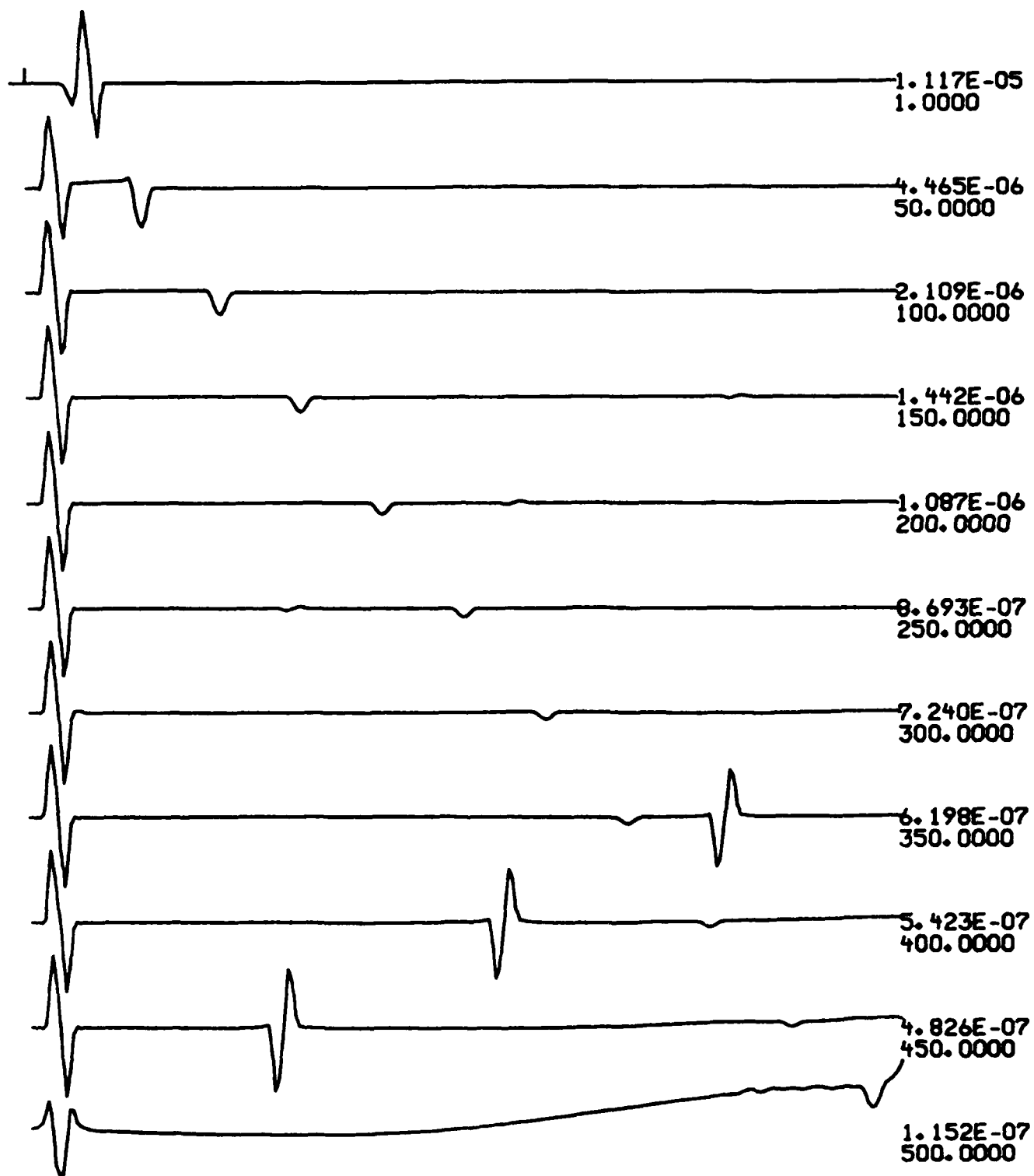


R-T JSRC=5 RELATIVE AMPLITUDE



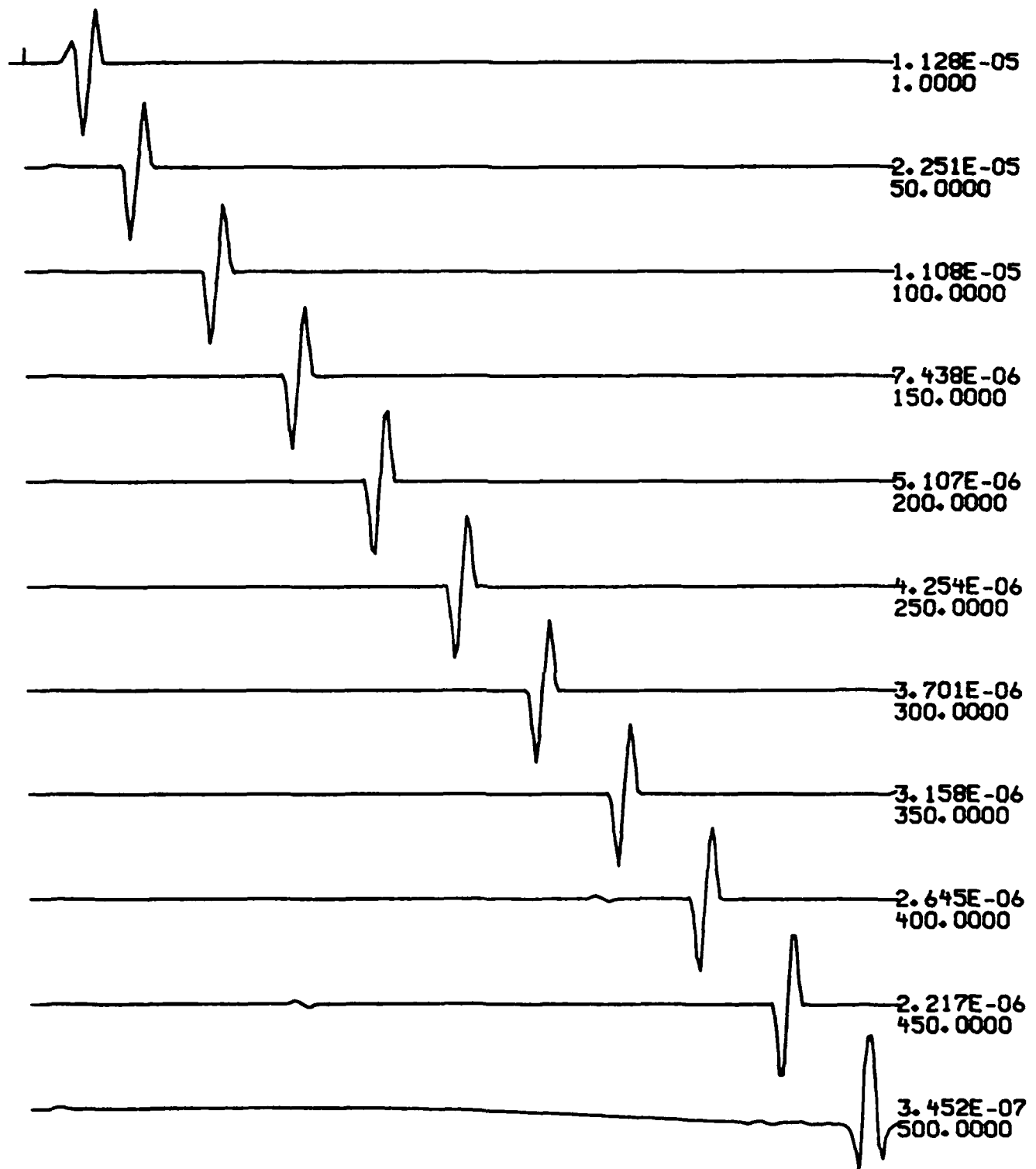
7

R-T JSRC=6 RELATIVE AMPLITUDE



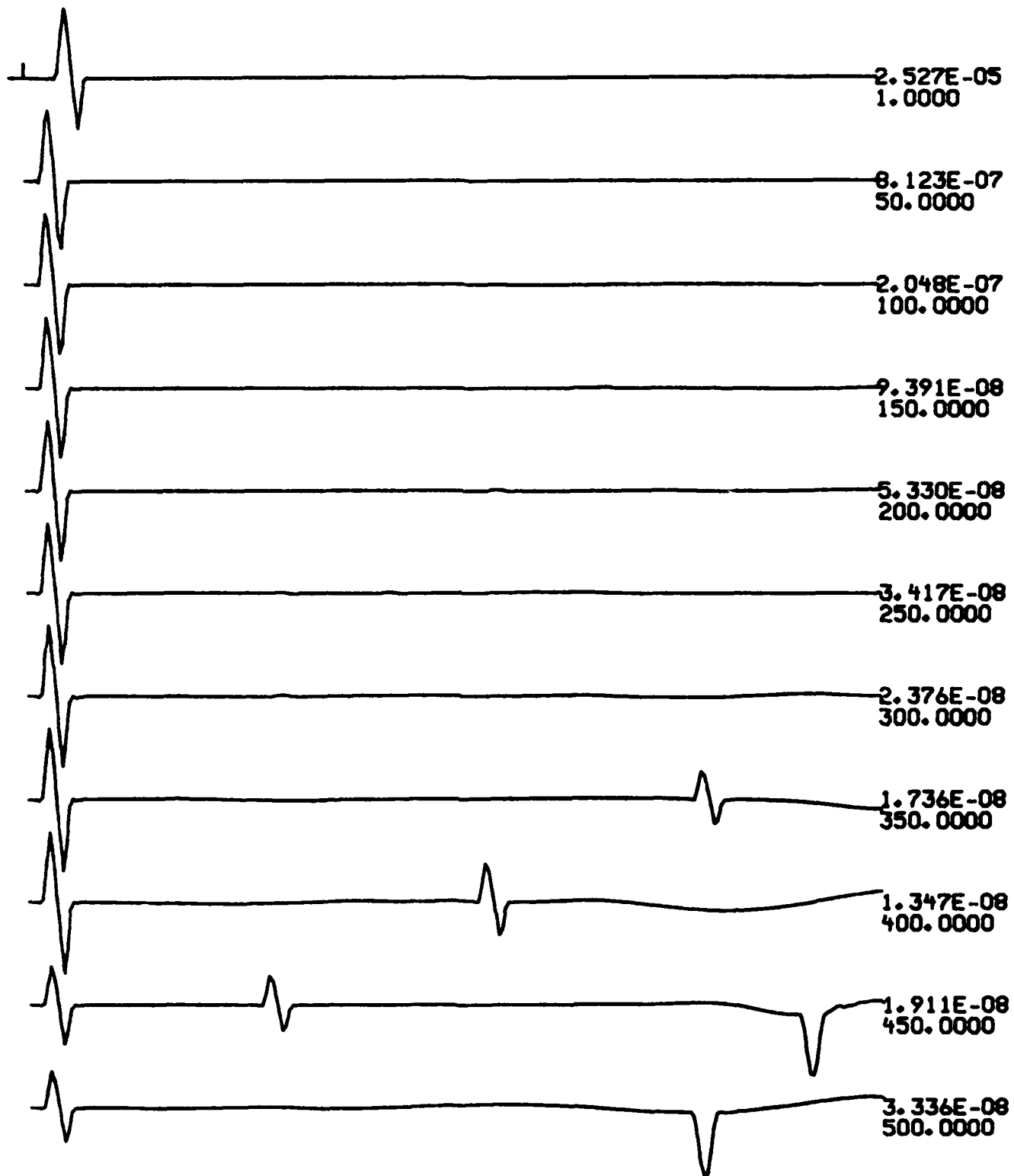
7

R-T JSRC=7 RELATIVE AMPLITUDE



7

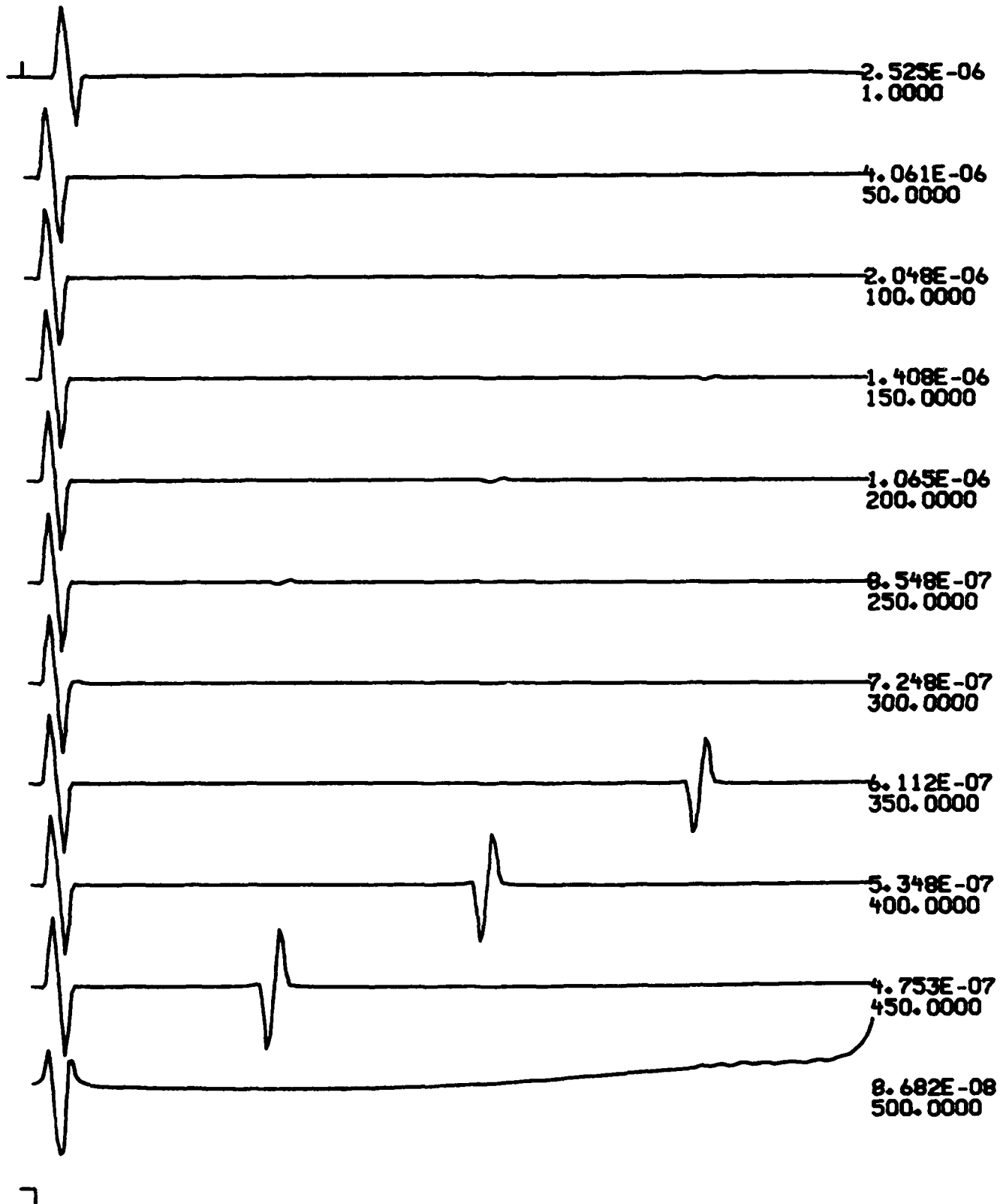
R-T JSRC=8 RELATIVE AMPLITUDE



7

R-T

JSRC=9 RELATIVE AMPLITUDE



R-T JSRC=10 RELATIVE AMPLITUDE

END

DTIC

8-86